

1 **Title Page**

2 **Single-cell transcriptomic atlas of individuals receiving inactivated COVID-19**
3 **vaccines reveals distinct immunological responses between vaccine and natural**
4 **SARS-CoV-2 infection**

5 Yi Wang ^{1,*}, Xiaoxia Wang ^{2,*}, Laurence Don Wai Luu ^{3,*}, Jieqiong Li ^{4,*}, Xiaodai Cui ¹, Hailan
6 Yao ⁵, Xin Zhang ⁶, Shaojin Chen ², Jin Fu ¹, Licheng Wang ², Chongzhen Wang ², Rui Yuan ²,
7 Qingguo Cai ², Xiaolan Huang ¹, Junfei Huang ⁷, Wenjian Xu ^{8,9,†}, Shijun Li ^{7,†}, Xiong Zhu ^{2,†}
8 and Jun Tai ^{10,†}

9 ¹ Experimental Research Center, Capital Institute of Pediatrics, Beijing, 100020, P.R. China

10 ² Central & Clinical Laboratory of Sanya People's Hospital, Sanya, Hainan 572000, P. R. China.

11 ³ School of Biotechnology and Biomolecular Science, University of New South Wales, Sydney,
12 Australia

13 ⁴ Department of Respiratory Disease, Beijing Pediatric Research Institute, Beijing Children's
14 Hospital, Capital Medical University, National Center for Children's Health, Beijing 10045, P. R.
15 China.

16 ⁵ Department of Biochemistry and Immunology, Capital Institute of Pediatrics, Beijing 100020, P.
17 R. China

18 ⁶ Beijing Engineering Research Center of Pediatric Surgery, Engineering and Transformation
19 Center, Beijing Children's Hospital, Capital Medical University, National Center for Children's
20 Health, Beijing 100045, P. R. China.

21 ⁷ Laboratory of Infectious Disease of Experimental Center, Guizhou Provincial Center for Disease
22 Control and Prevention, Guiyang 550050, P. R. China.

23 ⁸ Beijing Key Laboratory for Genetics of Birth Defects, Beijing Pediatric Research Institute,
24 Beijing Children's Hospital, Capital Medical University, National Center for Children's Health,
25 Beijing 10045, P.R. China.

26 ⁹ MOE Key Laboratory of Major Diseases in Children, Capital Medical University, Beijing 10045,
27 P.R. China.

28 ¹⁰ Department of Otolaryngology, Head and Neck Surgery, Children's Hospital Capital Institute of
29 Pediatrics, Beijing 100020, P. R. China.

30

31 [†] Correspondence:

32 Dr. **Yi Wang**, wildwolf0101@163.com (Handling the correspondence)

33 Dr. **Wenjian Xu**, xuwenjian85@qq.com

34 Prof. **Shijun Li**, zjumedjun@163.com

35 Prof. **Xiong Zhu**, zhuxiong6@163.com

36 Prof. **Jun Tai**, trenttj@163.com

37

38 * These authors contributed equally to this article

39

40 **Abstract**

41 To control the ongoing COVID-19 pandemic, CoronaVac (Sinovac), an inactivated
42 vaccine, has been granted emergency use authorization by many countries. However,
43 the underlying mechanisms of the inactivated COVID-19 vaccine-induced immune
44 response remain unclear, and little is known about its features compared to SARS-
45 CoV-2 infection. Here, we implemented single-cell RNA sequencing (scRNA-seq) to
46 profile longitudinally collected PBMCs (peripheral blood mononuclear cells) in six
47 individuals immunized with CoronaVac and compared these to the profiles of
48 COVID-19 infected patients from a Single Cell Consortium. Both inactivated
49 vaccines and SARS-CoV-2 infection drove changes in immune cell type proportions,
50 caused B cell activation and differentiation, and induced the expression of genes
51 associated with antibody production in the plasma. The inactivated vaccine and
52 SARS-COV-2 infection also caused alterations in peripheral immune activity such as
53 interferon response, inflammatory cytokine expression, innate immune cell apoptosis
54 and migration, effector T cell exhaustion and cytotoxicity, however, the magnitude of
55 change was greater in COVID-19 patients, especially those with severe disease, than
56 in immunized individuals. Further analyses revealed a distinct peripheral immune cell
57 phenotype associated with CoronaVac immunization (HLA class II upregulation and
58 *IL21R* upregulation in naïve B cells) versus SARS-CoV-2 infection (HLA class II
59 downregulation and *IL21R* downregulation in naïve B cells severe disease). There
60 were also differences in the expression of important genes associated with
61 proinflammatory cytokines and thrombosis. In conclusion, this study provides a
62 single-cell atlas of the systemic immune response to CoronaVac immunization and
63 reveals distinct immune responses between inactivated vaccines and SARS-CoV-2
64 infection.

65 **Keywords:** Inactivated vaccine, CoronaVac, COVID-19, SARS-CoV-2, Single-cell
66 sequencing, Immunological responses

67 **Introduction**

68 COVID-19 (coronavirus disease 2019), caused by SARS-CoV-2 (severe acute
69 respiratory syndrome coronavirus 2), is an unprecedented threat to global public
70 health and has rapidly spread throughout the world (Cevik et al., 2020). COVID-19
71 has led to high mortality and morbidity worldwide, and as of Aug 24, 2021,
72 213,752,662 laboratory-confirmed cases of SARS-CoV-2 infection have been
73 reported, resulting in 4,459,381 deaths (WHO COVID-19 Dashboard). As there are no
74 effective drugs available at this time against COVID-19, safe and effective COVID-
75 19 vaccines are urgently required to control the pandemic and reduce the global
76 burden of SARS-CoV-2 (Mehra et al., 2020).

77 Various candidate vaccines including inactivated viral vaccines, live attenuated
78 vaccines, nucleic acid vaccines, viral-vectored vaccines, and protein or peptide
79 subunit vaccines are being rapidly developed, tested, and granted approval for
80 emergency use (Amanat and Krammer, 2020). Each vaccine has advantages and
81 disadvantages and these have been reviewed elsewhere (Dong et al., 2020; Poland et
82 al., 2020). Among these candidate vaccines, the inactivated COVID-19 vaccines are
83 among one of the most widely used and well developed vaccines due to their ease of
84 production and scale-up, and relatively low cost. They are produced by growing
85 SARS-CoV-2 in cell culture (e.g., Vero cells), followed by chemical inactivation of
86 the virus (Krammer, 2020). Inactivated vaccines present the whole SARS-COV-2
87 virus for immune recognition, thus the immune responses are likely to target not only
88 the unique protein (e.g., S protein) of the virus but also matrix, nucleoprotein and
89 envelope (Krammer, 2020). Moreover, the inactivated vaccines exhibit stable
90 expression of conformation-dependent antigenic epitopes, and also offer advantages
91 in a variety of different populations (e.g., those with degrees of immune senescence)
92 (Iversen and Bavari, 2021b).

93 CoronaVac (initially known as PiCoVacc) from Sinovac, is a leading Chinese
94 COVID-19 vaccine and was devised with β -propiolactone as an inactivating agent and
95 formulated with aluminum hydroxide as an adjuvant (Gao et al., 2020). The

96 inactivated CoronaVac vaccine is a whole-virus preparation administered in a two-
97 dose regimen (at day 0 and day>21), and the immunogenicity, safety and tolerability
98 have been assessed in different populations, including children and adolescent aged 3-
99 17 years old (Han et al., 2021), adults aged 18-59 (Zhang et al., 2021), and adults
100 aged 60 years and older (Wu et al., 2021). Within the scope of combating the SARS-
101 CoV-2 pandemic, CoronaVac has been granted an emergency use authorization by
102 Chinese authorities in July, 2020 (Poland et al., 2020), and a host of others countries
103 such as Turkey, Chile, Brazil, Indonesia, etc. (Bayram et al.; Fortner and Schumacher,
104 2021; Muena et al., 2021; Shervani et al., 2020).

105 Currently, the knowledge about the immunity generated by COVID-19 vaccines
106 (including the inactivated vaccines) are limited with researchers understanding less
107 about this than about immunity to natural SARS-CoV-2 infection. Although clinical
108 trial data have demonstrated that the current COVID-19 vaccines approved (including
109 CoronaVac) can elicit immunity with a high degree of safety, efficacy and tolerability,
110 much remains to be learned concerning the genetic drivers of COVID-19 vaccine-
111 elicited humoral and/or cellular immunity, defining detailed targets of the immune
112 response at the epitope level, and characterizing the B-cell receptor and T-cell
113 receptor repertoire induced by COVID-19 vaccines (Poland et al., 2020). Inactivated
114 vaccines (such as CoronaVac) have been shown to keep the immunogenicity of the
115 SARS-CoV-2 virus, and can elicit an immune response, however whether there is a
116 distinct immune response landscape between natural SARS-CoV-2 infection and the
117 inactivated COVID-19 vaccine remains unclear.

118 Here, we implemented scRNA-seq (single-cell RNA sequencing) to obtain a
119 comprehensive and unbiased visualization of PBMCs (Peripheral blood mononuclear
120 cells) from healthy adults immunized with the inactivated COVID-19 vaccine,
121 CoronaVac, at 3 pivotal time points, including day 0 (before vaccination), day 21 after
122 the first dose and day 14 after the second dose (**Figure 1A**). This study provides a
123 high-resolution transcriptomic landscape of PBMCs during the immune response to
124 CoronaVac immunization, which will foster a better understanding of the protective

125 immune response generated by inactivated COVID-19 vaccines. Then, we compared
126 this data to the reported profiles from a Single Cell Consortium for COVID-19 (Ren
127 et al., 2021), revealing the distinct immune features between natural SARS-CoV-2
128 infection and the inactivated COVID-19 vaccine.

129

130 **Results**

131 **Single-cell transcription profiling of PBMCs**

132 To identify features of the immunological hallmarks from individuals receiving
133 inactivated COVID-19 vaccines (CoronaVac), the droplet-based scRNA-seq (10 X
134 Genomics) was conducted for studying the transcriptomic profiles of PBMCs, which
135 were longitudinally collected from six individuals at three pivotal time points (**Fig**
136 **1A**). Single-cell B cell receptor (BCR) and T cell receptor (TCR) sequencing were
137 also performed for each sample. According to the time points, these samples were
138 classified into three conditions: no injection (NJ, day=0, PMBCs were collected
139 before vaccination), first injection (FJ, Day=21, PMBCs were collected at day 21 after
140 the first dose) and second injection (SJ, Day=35 PMBCs were collected at day 14
141 after second dose). The associated metadata of the six individuals enrolled and the
142 three conditions are detailed in **Supplementary Table S1**. After the single-cell
143 analysis pipeline (Refer to Methods), we obtained ~0.895 billion unique transcripts
144 belonging to 178268 cells from the PBMCs of vaccinated individuals. Among these
145 cells, 60783 cells (34.1%) were from the NJ conditions, 47451 cells (26.6%) were
146 from the FJ condition, and 70034 cells (39.3%) from the SJ condition. Next, we
147 integrated all high-quality cells into an unbatched and comparable dataset, which was
148 subjected to principal component analysis after correction for read depth and
149 mitochondrial read counts (**Fig S1A-B**)

150 To reveal immune cell populations in individuals administered with inactivated
151 COVID-19 vaccines, the graph-based clustering of UMAP (uniform manifold
152 approximation and projection) was performed. According to the expression of
153 canonical cell-type markers, we identified 10 major cell types (**Fig 1B (left), C-D**;

154 **S1A-B**): B cells (CD79A⁺CD79B⁺MS4A⁺), plasma cells (XBP1⁺MZB1⁺), $\gamma\delta$ T cells
155 (TRDV1⁺TRDV9⁺), natural killer (NK) cells (CD11b⁺NKG7⁺KLRD1⁺NKG2A⁺),
156 CD4⁺ T cells (CD3D⁺CD3E⁺CD40LG⁺), CD8⁺ T cells (CD3D⁺CD3E⁺CD8A⁺CD8B⁺),
157 mucosal-associated invariant T (MAIT) cells (CD3D⁺CD3E⁺SLC4A10⁺), monocytes
158 (CST3⁺LYZ⁺CD68⁺), dendritic cells (CST3⁺LYZ⁺CD163⁺) and megakaryocytes
159 (CST3⁺LYZ⁺PPBP⁺). At the more granular level, we identified 27 different cell
160 subtypes (**Fig 1B (right), S1A-B**). Likewise, we also successfully identified 10 major
161 cell types (**Fig 1E (Left)**) and 27 cell subtypes (**Fig 1E (Right)**) for the PBMCs
162 samples reported by a Single Cell Consortium for COVID-19 (Ren et al., 2021) (**Fig**
163 **S1C-F**). As such, the composition of cell subpopulations in peripheral blood from
164 individuals with COVID-19 vaccine and COVID-19 patients were clearly defined
165 (**Fig 1B, E; S1G**).

166

167 **Differences in major cell type compositions across conditions**

168 We firstly uncovered the differences in cell composition (10 major cell types) across
169 two conditions (FJ and SJ) and then compared that with NJ. According to scRNA-seq
170 data (**Fig 2A-D**), we calculated the relative percentage of 10 major cell types in the
171 PBMCs of each participant at 3 conditions. The relative abundance of CD4⁺ T cells,
172 CD8⁺ T cells, $\gamma\delta$ T cells, NK cells and MAIT cells at FJ and SJ conditions remained
173 similar when compared with the NJ condition (**Fig 2D**). The relative percentage of B
174 cells appeared to increase in FJ and SJ conditions in comparison with NJ condition,
175 implying that the change in B cells may be related with the humoral immune response
176 after vaccination (**Fig 2D**). The proportions of dendritic cells (DCs), monocytes
177 (Mono) and megakaryocytes (Mega) increased after vaccination (**Fig 2D**). Increased
178 DCs may be involved in antigen presentation to stimulate the immune response to
179 CoronaVac, while increased Mono and Mega may be involved with the potential
180 inflammatory response after vaccination. Of note, the percentage of plasma cells did
181 not significantly increase in the FJ and SJ conditions (**Fig 2D**). This may be due to
182 plasma cells requiring a strong level of continuous antigen stimulation, or that the

183 plasma cell level had decreased or was restored when the PBMC samples were
184 collected at the FJ (at day 21 after first dose) and SJ (at day 14 after first dose)
185 conditions.

186 Next, we compared the cell composition between vaccine and natural SARS-
187 CoV-2 infection. Patients with COVID-19 (n=64) were classified into four conditions:
188 control (Cont; n=15), mild (mild; n=12), severe (seve; n=4) and convalescent (conv;
189 n=33) (**Fig 2E-G, Fig S2A**). After SARS-CoV-2 infection, the proportion of innate
190 immune cells, including NK cells, $\gamma\delta$ T cells, MAIT cells and DCs, decreased with
191 disease severity (**Fig 2E-G**). This trend was different to what was observed with
192 vaccines (**Fig 2D, G; S2B-D**). Similar with vaccination, the relative abundance of
193 monocytes and megakaryocytes in COVID-19 patients increased with disease severity,
194 and the relative percentage of these cells later declined in Conv conditions (**Fig 2G**).
195 Unlike the inactivated COVID-19 vaccine, a decrease in CD4⁺ T and CD8⁺ T cells
196 were observed in COVID-19 infected patients, and this was related with disease
197 severity (**Fig 2D, G; S2D**). A slight increase in B and plasma cell levels were
198 observed after SARS-CoV-2 mild infection, whereas a massive increase in plasma
199 cells was observed in the Seve condition (**Fig G; S2D**). These data suggested that
200 both vaccination with CoranaVac and natural SARS-CoV-2 infection can cause
201 changes in the cell compositions of PBMC.

202

203 **Features of B cell subsets across samples**

204 To reveal the dynamic changes in different B cell subtypes in immunized (**Figure 3A-**
205 **E, Fig S3A**) and infected individuals (**Fig 3F-G, S3B-E**), we classified B cells into 6
206 subsets according to the distribution and expression of classical subtype markers. We
207 successfully identified one naïve B subcluster (MS4A1⁺IGHD⁺), one memory B
208 subcluster (MS4A1⁺CD27⁺), one germinal center B subcluster (MS4A1⁺NEIL1⁺), one
209 intermediated transition memory B subcluster (Intermediate memory B,
210 MS4A1⁺IGHD⁺CD27⁺), one plasma B subcluster (MZB⁺CD38⁺) and one
211 proliferating plasma B subsets (MZB⁺CD38⁺MKI67⁺).

212 The general patterns of B/plasma cells were compared across conditions. The
213 relative percentages of an active state B subtype (germinal center B) significantly
214 increased after vaccination, suggesting that B cells may be activated after vaccination
215 (**Fig 3E**). Other B cell subsets, including naïve B cells, memory B cells and
216 intermediate memory B cells, remained similar across the three vaccination conditions
217 (NJ, FJ and SJ) (**Fig 3E**), suggesting that the inactivated COVID-19 vaccine has a
218 relatively low impact on the composition of these B cell subsets. Likewise, SARS-
219 CoV-2 infection also had relatively low impact on the composition of these B cell
220 subsets, with only the memory B subtype decreased in severe COVID-19 patients
221 (**Fig 3G**). Increased plasma and dividing plasma cells were observed in COVID-19
222 patients with the percentage of plasma cells in severe COVID-19 patients reaching 15%
223 while mild COVID-19 patients only reached 3% (**Fig 3G**) (Ren et al., 2021),
224 suggesting that antibody production may be stronger in severe COVID-19 patients,
225 reminiscent of previous findings that higher antibody titers are related with worse
226 clinical outcomes (Long et al., 2020; Okba et al., 2020). Although the levels of plasma
227 cells and dividing plasma cells did not significantly increase after vaccination, the
228 levels of neutralizing antibodies (anti-S-RDB-specific antibody) did significantly
229 increase after the second injection for all 6 individuals (**Fig 3H, Fig S3G, Table S2**).
230 Interestingly, the levels of neutralizing antibody did not significantly increase after the
231 first dose of CoronaVac (**Fig 3H, Fig S3G, Table S2**) and significant production of
232 neutralizing antibody was only obtained after the second dose. This implies that two
233 doses of CoronaVac are required for efficient seroconversion.

234 After vaccination, the plasma cells in PBMCs had highly expressed genes which
235 encode the constant regions of immunoglobulin G1 (Ig G1), IgG2, IgA1 or IgA2. This
236 correlates with their function in secreting antigen-specific antibodies and implies that
237 the serum of immunized individuals may have had high titers of SARS-CoV-2-
238 specific antibodies (**Fig 3H-I, S3G**). These findings were also observed in COVID-19
239 patients (**Fig 3J**), and is consistent with previous studies showing high titers of
240 antigen-specific antibodies in the serum of COVID-19 patients (Ni et al., 2020; Ren et

241 al., 2021). Similar to natural SARS-CoV-2 infection, genes encoding IgA1 and IgA2
242 were activated by CoronaVac, and this finding has also been observed in influenza
243 vaccines (Neu et al., 2019).

244

245 **Transcriptomic changes in B cells after vaccination and SARS-CoV-2 infection**

246 To investigate differential transcriptomic changes in B/plasma cells after vaccination,
247 we compared the expression profiles of B/plasma cells in FJ or SJ conditions with the
248 NJ condition. As expected, genes involved in B cell activation, adaptive immune
249 response, response to interferon, and antigen processing and presentation were
250 specifically enriched in B cells after vaccination (**Fig 4A**). This suggests that the B
251 cells were responding to the inactivated COVID-19 vaccine. For SARS-CoV-2
252 infection, genes involved in defense response to virus and interferon signaling
253 pathways were the most highly upregulated in the B cell subset (**Fig S4A**). Notably,
254 we observed that genes associated with the “IFN response” were enriched in both
255 post-vaccination samples and COVID-19 patients (**Fig 4A** and **Fig S4A**).

256 Next, we further examined the expression of important genes (e.g., *PRDMI*, T-
257 bet) that are involved in B/plasma-cell-activation-related processes after vaccination
258 and SARS-CoV-2 infection. Two GO pathways (GO:0002312 and GO:0042113) that
259 were related to the activation of B cells were significantly enriched after vaccination
260 (**Fig 4B**). Several genes (e.g., *PTPRC*, *HMCES* and *SWAP70*) involved in the B cell
261 activation GO pathways (GO:0002312 and GO:0042113), were highly upregulated in
262 the naïve B cell subtype, implying activation of naïve B cells after vaccination (**Fig**
263 **4C**). In contrast, these three genes (*PTPRC*, *HMCES* and *SWAP70*) were down-
264 regulated in severe COVID-19 patients, suggesting that activation of naïve B cells in
265 these individuals may be impaired (**Fig S4B**). Naïve B cells in vaccinated samples
266 also highly expressed *IL4R* and *IL21R* (**Fig 4D**), but these genes were downregulated
267 in activated and memory B cells (**Fig 4E**). This indicates that naïve B subsets were
268 more responsive than activated and memory B cells to IL-4 (interleukin 4) and IL-21,
269 which regulate class switching to IgG, including IgG1, IgG3 or IgG4 (Horns et al.,

270 2020; Pène et al., 2004). Similar findings for *IL4R* and *IL21R* expression were also
271 observed in SARS-CoV-2 mild infection, while *IL4R* and *IL21R* were significantly
272 downregulated in severe COVID-19 patients (**Fig S4C-D**).

273 Six transcription factors (TBX21, ZEB2, TFEC, ZBTB32 and YBX3) associated
274 with the activation of memory B cells were highly expressed in intermediate transition
275 memory B cell (also referred to as activated memory B cells) compared to memory B
276 cells (**Fig 4F** and **Fig S4E**) (Horns et al., 2020). TBX21 (also known as T-bet) has
277 been hypothesized to play a key regulatory role in activation and is required for class
278 switching to IgG2 (Wang et al., 2012). This transcription factor showed higher
279 expression in activated memory B cells than memory B cells (**Fig 4F** and **Fig S4E**). A
280 triad of transcription factors, including PRDM1, XBP1 and IRF4, also had increased
281 expression in activated B cells (which encompasses: germinal center B cell,
282 intermediate transition memory B cell, dividing plasma and plasma) from COVID-19
283 patients and immunized individuals than non-activated B cell (including naïve B cell
284 and memory B cell) (**Fig 4G** and **Fig S4F**). These transcription factors are associated
285 with B-cell-differentiation-related pathways and are required for activating the ASC
286 (antibody-secreting cell) program (Shi et al., 2015). PRDM1 plays a core role in
287 determining and shaping the secretory arm of B cell differentiation and in promoting
288 Ig synthesis. XBP1 is a positively acting transcription factor of the CREB-ATF family
289 that is highly express in plasma cells and is important for increasing protein synthesis
290 in plasma cells (Shaffer et al., 2004). IRF4 is crucial for regulating Ig class-switch
291 recombination, and a previous study has found that sustained and increased
292 concentration of this transcription factor promotes the generation of plasma cells
293 (Ochiai et al., 2013). Finally, three B cell-promoting transcription factors: BACH2,
294 BCL6 and PAX5, showed increased expression in B cells after vaccination (**Fig 4H**)
295 while in severe COVID-19 patients (**Fig S4G**), these transcription factors decreased.
296 BACH2, BCL6 and PAX5 play a key role in determining the fate of B cells during
297 differentiation (Shi et al., 2015).

298 Interestingly in COVID-19 infected samples, expression of important chemokine

299 receptors such as CXCR5 were significantly decreased, especially for severe samples
300 (**Fig S4H**). However, this loss of chemokine receptors was not observed in
301 immunized samples (**Fig 4I**). Decreased chemokine receptors can impair germinal
302 center reactions and ultimately cause dysregulated humoral immunity responses
303 (Mathew et al., 2020; Okada et al., 2002; Reimer et al., 2017). Our data also observed
304 significant upregulation of HLA class II genes after immunization (**Fig 4J**), implying
305 that there is an enhancement of immune cell crosstalk between the adaptive immune
306 cell classes. However in COVID-19 patients, several HLA class II genes were
307 significantly downregulated, especially for severe COVID-19 patients (**Fig S4I**). This
308 suggests a dysregulation of immune cell crosstalk between the adaptive immune cell
309 classes during infection. Together, these data define the transcriptional hallmarks of
310 CoronaVac-induced B cell activation and clonal expansion and revealed underlying
311 differences in the B cell transcriptome between vaccine-induced immunity and SARS-
312 CoV-2 infection.

313

314 **V(D)J gene usage and clonal expansion in B cells after vaccination and SARS-** 315 **CoV-2 infection**

316 BCR information was detected in all B/plasma subsets and in >80% of cells while
317 clonal expansion (clonal size >10) was observed in memory B cells, intermediate
318 transition memory B cells, dividing plasma cells, and plasma cells (**Fig 5A, Fig S5A-**
319 **B**). The largest proportion of BCR in B cells was the IGHM subtype and the largest
320 proportion of BCR in plasma cells were IGHA1 and IGHG1 (**Fig 5B**). After
321 vaccination, the percentage of IGHM significantly increased in B cells (**Fig 5C, Fig**
322 **S5A**) while the percentage of IGHA1 decreased in plasma cells (**Fig 5C, S5C, S5D**).
323 The light chain type, IGK and IGL, did not change in B and plasma cells (**Fig 5D**).

324 We compared the clonal expansion of B cell subtypes under different conditions
325 in the vaccine cohort (**Fig 5E**). BCR clonal expansion of plasma cells increased from
326 NJ to FJ to SJ, suggesting that two-doses of CoronaVac induced plasma proliferation
327 of specific BCR clonotypes. In COVID-19 patients, increased clonal expansion in

328 CD8⁺ T was also observed in severe COVID-19 patients (**Fig 5E**), in agreement with
329 Zhang et al. (Zhang et al., 2020).

330 BCR diversity, as measured by alpha diversity, showed no change after
331 vaccination but was significantly decreased in severe COVID-19 infections (**Fig 5H**).
332 The length distribution of the CDR3 region was similar for all conditions except
333 COVID-19 severe condition (**Fig5I**). These results suggest that vaccine induced
334 immune protection in very gentle way.

335 The usage of IGH V(D)J genes across vaccination and infection conditions were
336 compared (**Fig 5F**). The combinations of the 6 IGHJ and >40 IGHV genes
337 demonstrated that CoronaVac induced many changes in the IGH V(D)J genes (**Fig 5F**
338 left panel). The V(D)J pair pattern were significantly altered after two doses of
339 CoronaVac. For example, the most prevalent pair in NJ was IGHJ2/IGHV3-23 which
340 shifted to IGHJ2/IGHV4-59 and IGHJ1/IGHV3-23 following vaccination. The
341 percentage of IGHJ1/IGHV3-43 and IGHJ1/IGHV3-15 also increased after
342 vaccination. In addition, we also analyzed the usage of IGK/L V(D)J genes (**Fig 5F**
343 right panel) and observed that the V(D)J pair pattern were also altered after two doses
344 of CoronaVac. For example, IGKJ5/IGKV3-11, IGLJ1/IGKV2-14 and IGLJ7/IGKV1-
345 51 were all increased after vaccination. Interestingly, IGLJ1/IGKV2-14 and
346 IGLJ7/IGKV1-51 were also increased in COVID-19 Mild and Conv conditions
347 compared to Cont. These results suggest a similarity in B-cell protective responses
348 between vaccine and Mild/Conv conditions.

349

350 **Characterization of innate immune cells**

351 To investigate vaccine (**Fig 6A-D, S6A**) and infection-driven (**Fig 6F, S6B-E**)
352 changes in innate immune cells, the distribution and expression of classical subtype
353 markers were used to classify innate cell types. We identified 6 innate cell types
354 including NK cells, $\gamma\delta$ T cells, MAIT cells, DC cells, monocytes and megakaryocytes
355 (**Fig 6A-B, 6F, S6A-E**). The dendritic cells were further classified into 2 subtypes
356 including pDCs, (plasmacytoid dendritic cells) and mDC (monocyte-derived dendritic

357 cells), while monocytes were classified into 3 subtypes including CD16⁺ monocytes,
358 CD14⁺ monocytes and CD14⁺CD16⁺ monocytes (**Fig 6A-B, 6F, S6A-E**).

359 To obtain further insights into the features of innate cells, we examined the
360 distribution of each subset across three conditions (NJ, FJ and SJ). The proportions of
361 $\gamma\delta$ T cells, NK cells, MAIT cells, CD16⁺ Mono, CD14⁺CD16⁺ Mono were similar
362 across the three conditions (NJ, FJ and SJ) (**Fig 6E, 6H, S6F**), while the relative
363 percentages of $\gamma\delta$ T cells, NK cells and MAIT cells decreased after SARS-CoV-2
364 infection, especially in severe patients (**Fig 6G, 6H, S6F**). The innate cell subsets
365 mDC, pDC, megakaryocytes and CD14⁺ monocytes increased after vaccination (**Fig**
366 **6E, 6H, S6F**). For COVID-19 patients, the percentages of mDC and pDC
367 significantly decreased in severe patients but were restored in convalescent samples
368 (**Fig 6G, 6H, S6F**). In contrast, the proportions of megakaryocytes and
369 CD14⁺ monocytes were significantly increased in severe patients and were also
370 increased in convalescent samples (**Fig 6G, 6H**). These findings of changes to innate
371 cell subsets in COVID-19 patients are consistent with previous reports and flow-
372 cytometry-based results (Jouan et al., 2020; Wilk et al., 2020). These data also
373 indicate that both vaccines and SARS-CoV-2 infection alter components of the innate
374 cells in PBMCs and reveals distinct differences in innate cells between vaccine-
375 induced immunity and natural SARS-CoV-2 infection.

376

377 **Transcriptomic changes in innate immune cells after vaccination and SARS-** 378 **CoV-2 infection**

379 Next, we investigated the transcriptomic changes in innate immune cells after
380 vaccination. GO (Gene Ontology) analyses were conducted to obtain functional
381 insights into innate cell subtypes between FJ/SJ conditions with NJ condition (**Fig**
382 **7A**). Genes associated with the adaptive immune response (such as “T cell activation”,
383 “immune response-activating signal transduction” and “antigen processing and
384 presentation”) were enriched after vaccination (**Fig 7A**), while for COVID-19
385 infection, other pathways (such as “response to virus” and “defense response to virus”)

386 were enriched (**Fig S7A**). Genes associated with “Response to IFN signaling” were
387 enriched in both vaccination and SARS-CoV-2 infection (**Fig 7A-B, S7B-7C**). INF
388 response is an essential pathway for innate cells to respond to viral infections, and our
389 data indicates that CoronaVac successfully induces the INF response in innate cells
390 (**Fig 7B, S7B**). The “INF response” of innate immune cells was stronger in SARS-
391 CoV-2 infection (especially for severe COVID-19 patients) compared to vaccination
392 (**Fig 7B**). We observed that four innate immune cell types (monocytes, $\gamma\delta$ T, MAIT
393 and NK cells) exhibited significantly upregulated IFN after vaccination (**Figure S7B**),
394 while all 6 innate cell types had higher IFN in COVID-19 patients (**Fig S7C**).

395 Our data showed that levels of cellular apoptosis and migration were
396 significantly upregulated in innate cells at the bulk level after vaccination and SARS-
397 CoV-2 infection (**Fig 7C, S7D-E**). The expression of HLA-II genes at FJ and SJ
398 conditions was higher compared to NJ, suggesting the enhancement of crosstalk
399 across cells after vaccination (**Fig 7E**). However, some HLA-II genes (e.g., *HLA-*
400 *DRB5*, *HLA-DPBI* and *HLA-DPA1*) were downregulated after SARS-CoV-2 infection,
401 especially in severe COVID-19 patients (**Fig 7F**), implying possible impairment of
402 crosstalk across cells. Genes which encoded HLA class I molecules (such as HLA-A,
403 HLA-B and HLA-E) were upregulated in innate cells from immunized samples
404 relative to NJ condition (**Fig S8**). Similar results were also seen in COVID-19 patients
405 (**Fig S9**). The underlying mechanism and effect of changes in HLA-I molecules
406 requires further investigation. In addition, we also investigated the expression of
407 several critical genes related with platelet aggregation (P2RX1, P2RY1 and TBXA2R)
408 in megakaryocytes (Sanguhl et al., 2011). P2RX1, P2RY1 and TBXA2R were not
409 significantly upregulated after immunization which suggests a low risk of thrombosis
410 following CoronaVac immunization (**Fig 7G**). P2RX1, P2RY1 and TBXA2R were
411 significantly upregulated in mild COVID-19 patients (**Fig 7G**), which may imply a
412 higher risk of thrombosis for mild COVID-19 patients than severe COVID-19 patients.
413 We further analyzed monocytes, as previous reports suggested that this cell
414 subset appeared to be the source of inflammation in COVID-19 patients (Ren et al.,

415 2021). We evaluated the expression of genes reported to encode inflammatory
416 cytokines (**Table S3**) (Ren et al., 2021; Wilk et al., 2020). We found elevated
417 expression of inflammatory genes in COVID-19 patients compared to healthy controls
418 at the bulk level, indicating that peripheral monocytes are potential contributors to the
419 inflammatory cytokine storm observed in COVID-19 patients. However, severe
420 COVID-19 patients did not show higher expression of inflammatory cytokines
421 compared to mild patients (**Fig I**). We also identified increased expression of
422 inflammatory response genes in vaccinated individuals (FJ and NJ conditions)
423 compared to NJ condition at the bulk level, especially after the second dose (**Fig 7J**).
424 Of note, expression of inflammatory response genes in vaccinated individuals was
425 much lower than COVID-19 patients (**Fig K**). This implies that post-vaccination may
426 not cause an increase in inflammatory cytokines in peripheral blood or causes a lower
427 increase in inflammatory cytokines. To validate this result, we investigated the levels
428 of 11 cytokines (including pro-inflammatory cytokines: TNF- α , IL-1B and IL-6) in the
429 sera of the 18 samples using a bead-based flow-cytometry assay on the BD
430 LSRFortessa X-20 platform. No obvious post-vaccination elevation in most cytokines
431 were observed (**Fig S10**), which further suggests that post-vaccination does not lead
432 to significant increases in inflammatory cytokines in peripheral blood. Interestingly,
433 CD14⁺monocytes contributed to the highest proportion of cell composition (**Fig 7L**)
434 and inflammatory scores (**Fig 7M**) after vaccination or SARS-CoV-2 infection,
435 suggesting that CD14⁺ monocytes may be the major source of inflammation (Ren et
436 al., 2021; Zhou et al., 2020).

437

438 **Features of T cell subsets in individuals after vaccination and SARS-CoV-2** 439 **infection**

440 To investigate changes in individual T cell subclusters, the T cells from PBMCs of
441 vaccinated individuals across three conditions (NJ, FJ and SJ) (**Fig 8A-B, S11A**) and
442 in COVID-19 patients (**Fig S11B-D**) were subclustered into 12 subtypes according to
443 the distribution and expression of classical T cell markers. These include 7 CD4⁺T

444 cell subtypes (CD3D⁺ CD3E⁺ CD40LG) and 5 CD8⁺T cell subtypes (CD3D⁺ CD3E⁺
445 CD8A⁺CD8B⁺).

446 For CD4⁺T cells, we defined one naïve CD4⁺ T cell subset (CCR7+SELL+), one
447 memory CD4⁺ T cell subset (S100A4⁺GPR183⁺), one effector memory CD4⁺ T cell
448 subset (S100A4⁺GPR183⁺GZMA⁺), one regulatory CD4⁺ T cell subset (T_{reg};
449 FOXP3⁺IL2RA⁺), one follicular T helper (Tfh) cell subset (CXCR5⁺, ICOS⁺,
450 SLAMF1⁺) and two effector CD4⁺ T cell subsets (CD4⁺ effector-GZMK and CD4⁺
451 effector-GNLY). Notably, the CD4⁺ effector-GNLY cell subtype was characterised
452 with high expression of genes related with cytotoxicity, such as *GNLY*, *GZMB*, *NKG7*
453 and *KLRD1*, whereas the CD4⁺ effector-GZMK cell subtype displayed high
454 expression of *GZMK* and low expression of other cytotoxic genes (**Fig 8A-B, S11A,**
455 **Table S5**). The CD4⁺ effector-GNLY subtype also had highly expressed TBX-21 (T-
456 bet), suggesting that this subcluster were Th-1 (Type 1 helper)-like cells (**Table S5**).
457 For CD8⁺ T cells, we defined one naïve CD8⁺ T cell subset (CCR7⁺SELL⁺), one
458 cycling CD8⁺ T cell subset (MKI67⁺), one effector memory CD8⁺ T cell subset
459 (S100A4⁺GPR183⁺GZMA⁺), two effector CD8⁺ T cell subsets (CD8⁺ effector-GNLY
460 and CD8⁺ effector-GZMK) (**Fig 8A-B, S11A, Table S5**).

461 To gain further insights into the characteristics of the T cell subclusters, we
462 examined the distribution of each subtype across three vaccine timepoints (**Fig 8C-E**)
463 and compared these profiles with data collected from COVID-19 patients (**Fig 8F,**
464 **S11E-G**). Three T cell subsets were significantly altered after vaccination (**Fig 8E**) in
465 comparison to NJ with CD4⁺ effector-GNLY and Tfh cell subsets decreasing while
466 Treg cells increased. For SARS-CoV-2 infection, the relative percentage of naïve
467 CD8⁺ T cells significantly decreased in severe COVID-19 patients whereas no
468 significant changes were observed in naïve CD4⁺ T cell subsets (**Fig 8F**). The
469 proportion of CD4⁺ effector memory decreased in COVID-19 patients compared to
470 controls (**Fig 8F**) and in the convalescence stage, the CD4⁺ effector memory cells
471 remained low and were not restored to the levels observed in the controls. In contrast,
472 two cytotoxic subsets, including CD4⁺ effector-GNLY and CD4⁺ effector-GZMK,

473 were present in higher percentages for convalescence patients (**Fig 8F**). Of particular
474 note, the cycling CD8+ subset was almost absent in controls but were highly enriched
475 in COVID-19 patients, especially for severe patients (**Fig 8F**). Besides naïve CD8+,
476 CD4+ effector-GNLY, CD4+ effector-GZMK, CD4+ effector memory and cycling
477 CD8+ subsets, others T cell subsets were not significantly altered (**Fig 8F, S11F-G**).

478

479 **Transcriptomic changes in T cells after vaccine and SARS-CoV-2 infection**

480 We investigated transcriptomic changes in the T cell subsets of vaccinated participants
481 and identified differences between vaccine and natural infection induced responses.
482 GO analyses found that genes associated with “T cell activation”, “antigen processing
483 and presentation” and “response to interferon” were enriched in T cell subsets after
484 vaccination, implying an ongoing adaptive immune response to vaccination (**Fig 9A**).
485 For SARS-CoV-2 infection, “Interferon signaling pathway”, “response to virus” and
486 “defense response to virus” were specifically enriched in T cell subsets, suggesting an
487 ongoing response against the virus (**Fig S12A**). IFN response is essential to the
488 immune response triggered by vaccines or viral infections and consistently, we found
489 that T cell subsets exhibited significant upregulation of IFN after vaccination and
490 SARS-CoV-2 infection (**Fig 9B, S12B**). Four activated state T cell subsets, including
491 CD4+ effector memory, CD4+ effector-GZMK, CD8+ effector-GNLY and CD8+
492 effector memory, showed significantly upregulated IFN after vaccination, whereas in
493 SARS-CoV-2 infection, all activated state T cell subsets had IFN significantly
494 upregulated (**Fig 9C, S12B**). COVID-19 patients had stronger expression of IFN than
495 vaccinated individuals (**Fig 9D**).

496 We then evaluated the cytotoxicity scores of different effector T cell subsets after
497 vaccination. Our data showed that effector T cell subsets had lower cytotoxicity
498 scores after vaccination than NJ condition at the bulk level (**Fig 9E**), and only two
499 effector T cell subsets (CD8+ effector-GNLY and CD8+ effector memory) showed
500 higher cytotoxicity scores after vaccination (**Fig 9F**). In contrast, the effector T cell
501 subsets exhibited higher cytotoxicity scores in COVID-19 patients than controls at the

502 bulk level, and all effector T cell subsets showed higher cytotoxicity scores in
503 COVID-19 patients (**Fig S12C**). COVID-19 patients also exhibited higher
504 cytotoxicity scores than vaccinated individuals (**Fig 9G**). Interestingly, we did not
505 observe significant elevation in exhaustion scores for effector T cell subsets after
506 vaccination at the bulk level (**Fig 9H**) however only CD4⁺ effector-GNLY and CD8⁺
507 effector-GZMK showed an increase in exhaustion scores after vaccination (**Fig 9I**).
508 For SARS-CoV-2 infection, effector T cell subsets did show higher exhaustion scores
509 at the bulk level (**Fig S12D**). All effector T cell clusters in mild and severe COVID-19
510 patients had higher exhaustion scores than controls, with severe patients having the
511 highest exhausted score (**Fig 9J, S12D**). COVID-19 infection did not displayed a
512 stronger exhaustion score in comparison to vaccinated individuals (**Fig 9J**).

513 We also investigated the apoptosis and migration scores of different T cell subsets.
514 Our data indicated that both vaccination and SARS-CoV-2 infection showed a high
515 level of apoptosis and migration in T cell subsets at the bulk level (**Fig 9K-P, S12E-**
516 **F**), however stronger apoptosis and migration of T cell subsets were observed in
517 COVID-19 patients, especially in the severe group (**Fig 9K-P, S12E-F**). These results
518 suggest that significant activation of cell apoptosis and migration pathways in the
519 PBMCs of severe disease may be associated with lymphopenia, consistent with
520 previous studies (Chen et al., 2020; Tan et al., 2020).

521 In addition, we observed that the expression of CD2AP significantly upregulated on
522 activated CD4⁺ T cells after vaccination and SARS-CoV-2 infection (**Fig 9Q**).
523 CD2AP, as an adaptor protein in CD4⁺ T cell, can modulate the differentiation of Tfh
524 cells and promote protective antibody responses in viral infection (Raju et al., 2018).
525 The expression of CD258 (TNFSF14) also significantly upregulated on activated
526 CD4⁺ T cells (**Fig 9R**) and cytotoxic CD8⁺ T cells (**Fig 9T**) after vaccination and
527 SARS-CoV-2 infection. TNFSF14 serves as a key component for T cell recruitment to
528 tissues from peripheral blood as well as promote T cell activation. The expression of
529 KDM5A significantly elevated in cytotoxic CD8⁺ T cells after vaccination and
530 SARS-CoV-2 infection (**Fig 9S**). KDM5A encodes a demethylase-H3K4me3, which

531 is needed for T cell activation. These data suggested that increased activation of T
532 cells in vaccinated individuals and COVID-19 patients may contribute to defense
533 against the vaccine and SARS-CoV-2 virus.

534

535 **V(D)J gene usage and clonal expansion in T cells after vaccination and SARS-** 536 **CoV-2 infection**

537 TCR information was detected in all subsets and in ~60% of T cells. Clonal expansion
538 of CD8+ effector T cells was larger (clonal size >100) than CD8+ cycling T cells and
539 CD4+ T cells (**Fig10A-B**). >70% of T cells in the vaccine cohort and 53%~61% of T
540 cells in COVID-19 cohorts had unique TCR clonotypes (**FigS13A-B**). A negative
541 correlation between clone size and clonotype number was observed, consistent with
542 previous report (Zhang et al., 2020) and suggests that large clonal expansion is a rare
543 event (**Fig 10C**). Next, we compared the expression of T cell receptor β -chain
544 constant domains 1 and 2 (TRBC1 and TRBC2). The percentage of TRBC1 increased
545 after vaccination, while in COVID-19 patients, the percentage of TRBC1 was highest
546 in severe disease and lowest in controls (**Fig 10D, H, S13C**). This suggests that
547 immune activation by vaccination and infection are able to modulate T cell receptor β -
548 chain ratios.

549 We compared T cell clonal expansion after vaccination and observed a
550 significant decrease in clonal expansion of CD8+ T cells, especially CD8+T effector-
551 GNLV cells, from NJ to FJ to SJ. This suggests that two-doses of CoronaVac induced
552 immunogenic proliferation leading to many new unique TCR clonotypes (**Fig 10E,**
553 **S13D**). For COVID-19 infection, decreased CD8+ T cell clonal expansion was also
554 observed in infected patients compared to Cont and Conv (**Fig 10E**), in agreement
555 with previous report (Tanriover et al., 2021). Clonal expansion in CD4+ T cells was
556 also decreased from NJ to SJ but was higher in severe than controls, suggesting that
557 CD4+ T cells may play different roles in vaccine and infection immune responses
558 (**Fig 10E**).

559 The length distribution of the CDR3 region were similar for all conditions

560 (Fig10G). COVID-19 infected patients tended to have lower TCR diversity while
561 vaccinated patients had higher diversity (Fig 10I) which may suggest a protective role
562 for TCR diversity. The usage of TRB V(D)J genes across vaccine and infection
563 conditions were compared (Fig 10F). The combination of the most prevalent 11 TRBJ
564 and 22 TRBV genes indicates that vaccination induced greater diversity in TRB
565 V(D)J genes (Fig10F top panel). Mild COVID-19 infection also induced greater
566 diversity however no new V(D)J pair patterns were observed. In contrast, severe
567 COVID-19 infection induced new prominent V(D)J pairs, including TRBJ1-6/TRBV9,
568 TRBJ1-4/TRBV27 and TRBJ1-5/TRBV4-1. The change in pattern for TRAJ and
569 TRAV pairs showed similar trends to TRB V(D)J (Fig10F bottom panel). In addition,
570 the CDR3 peptides sequences showed large individual differences however we did not
571 observe any interesting patterns across conditions (Fig S14).

572

573 Discussion

574 As an emerging virus, SARS-CoV-2 is highly pathogenic and is responsible for the
575 COVID-19 pandemic. Currently, there are no effective drugs or optimal treatments for
576 SARS-CoV-2 infection, thus considerable effort has been put into developing safe and
577 effective vaccines against COVID-19. Inactivated SARS-CoV-2-based vaccines are
578 one of the most-widely used COVID-19 vaccines due to its low cost, ease of scale-up
579 and production (Iversen and Bavari, 2021a). CoronaVac is an inactivated COVID-19
580 vaccine candidate which has had its safety and potency validated in both animal
581 models and clinical trials (Tanriover et al., 2021; Zhang et al., 2021). However,
582 current knowledge of the host immune response to the inactivated COVID-19 vaccine
583 is still limited, making it difficult to inform and improve the design of new
584 generations of COVID-19 vaccines. In addition, little is known about how this
585 immune response compares to natural SARS-CoV-2 infection.

586 In this report, we performed single-cell RNA sequencing in PBMCs of six
587 individuals immunized with CoronaVac and compared these to the single-cell profiles
588 in COVID-19 patients. Overall, both inactivated SARS-CoV-2 vaccine and natural

589 SARS-CoV-2 infection affect the composition of peripheral immune cells, with
590 greater changes observed in COVID-19 patients, especially for severe disease. After
591 CoronaVac injection, the inactivated SARS-CoV-2 virus initially encounters antigen
592 presenting cells (APCs) in the innate immune system which then triggers the adaptive
593 immune response. Our data confirmed that the proportion of DCs, one of the main
594 APCs, are significantly elevated after vaccination (**Fig 2**), thus suggesting that
595 CoronaVac is able to successfully initiate the adaptive immune response. However in
596 severe COVID-19 patients, the relative percentage of DCs significantly decreased,
597 implying a possible subversion of the adaptive immune response in severe disease.
598 Monocytes are the major source of inflammatory cytokines in SARS-CoV-2 infection
599 (Ren et al., 2021; Zhou et al., 2020), and were elevated after immunization with
600 CoronaVac and SARS-CoV-2 infection (**Fig S2**). However, the level of monocytes
601 was significantly greater in COVID-19 patients (especially for severe disease)
602 compared to immunization. This implies that CoronaVac immunization causes a
603 weaker inflammatory response than natural SARS-CoV-2 infection. The relative
604 abundance of $\gamma\delta$ T, MAIT, NK, CD4+ effector memory, and naïve CD8+ T cells
605 decreased with disease severity while the proportion of cycling CD8+ T cells
606 increased with disease severity, suggesting that these subsets may be associated with
607 disease severity. We did not observe significant changes to these subsets after
608 immunization with CoronaVac (**Fig 2, 6, 9, S2, S6 and S11**).

609 IFNs are produced during viral infection and has an antiviral role. However
610 when produced excessively, IFNs can cause immunopathological damages.
611 Interestingly, 'IFN response' was enriched by GO analysis in different cell subclusters
612 after vaccination in our study (**Fig 4, 7 and 9**). Compared to pre-vaccination samples,
613 the response to IFN- α (type I IFN) pathway was also significantly elevated in most
614 PBMC cell types in post-vaccination samples. Together, this suggests CoronaVac
615 induces IFNs as part of the antiviral response. Similarly, 'IFN response' was also
616 enriched by GO analysis after SARS-CoV-2 infection (**Fig S4, S7 and S12**). The
617 expression level of IFN- α was also significantly upregulated in COVID-19 patients

618 (Fig S4, S7 and S12), suggesting an antiviral role triggered by IFNs. Notably,
619 COVID-19 patients showed higher response to IFN- α than immunized individuals
620 with the strongest response to IFN- α found in severe disease (Fig 7, 9). This indicates
621 that the stronger response to IFNs in COVID-19 patients may be involved in immune
622 pathology (e.g., lung injury) (Liu et al., 2020).

623 In this report, we observed broad immune activation after immunization with
624 CoronaVac. First, the levels of neutralizing antibodies (anti-S-RDB-specific antibody)
625 significantly increased after the second injection (Fig 3, S3, Table S2). Second, B cell
626 activation in PBMCs post-vaccination is supported by our data and evidenced by: (i)
627 enrichment of genes involving in ‘B cell activation’, ‘adaptive immune response’ and
628 ‘antigen processing and presentation’; (ii) significant upregulation of two important B
629 cell activation pathways (GO:0002312 and GO:0042113); (iii) the activation of naïve
630 B and memory B cell subsets; (iv) significant expression of key genes (e.g., *PRDM1*,
631 *XBPI*, *IFR4*, *PAX5*, *IL4R* and *IL21R*). Third, the activation of innate immune cells
632 was observed in our study as genes associated with ‘antigen processing and
633 presentation’, ‘IFNs response’, ‘T cell activation’ and ‘immune response-activating
634 signal transduction’ were enriched by GO analysis (Fig 7). Fourth, the activation of T
635 cell subsets was also supported by our data as genes involved in ‘T cell activation’, ‘T
636 cell mediated immunity’, ‘antigen processing and presentation’, and ‘IFNs response’
637 were also enriched by GO analysis (Fig 9). Similarly, broad immune activation was
638 also observed after SARS-CoV-2 infection (Fig S4, S7, S12). However, we observed
639 significant downregulation of some HLA class II genes in B, T and innate cells in
640 COVID-19 patients, especially for severe disease, implying a dysregulation in
641 crosstalk between adaptive immune cell classes. Furthermore, some key chemokine
642 receptor genes (e.g., *CXCR5*) were also significantly downregulated in the PBMCs of
643 severe COVID-19 patients (Fig S4), which may impair germinal center reaction,
644 resulting in a dysregulated humoral immune response (Mathew et al., 2020).

645 We analyzed the apoptosis, migration, cytotoxicity and exhaustion scores in
646 different immune cell subsets from immunized individuals and compared their

647 expression levels with COVID-19 patients. Overall, innate immune and T cell subsets
648 showed higher apoptosis and migration scores after immunization with CoronaVac or
649 SARS-CoV-2 infection (**Fig 7, 9, Fig S7 and S12**). However, compared to post-
650 vaccination, SARS-CoV-2 infection exhibited higher apoptosis and migration scores,
651 with severe disease having the highest score. This suggests that severe patients likely
652 had increased lymphocyte apoptosis and migration which may be associated with
653 lymphopenia, a clinical predictor for severe COVID-19 disease (Tan et al., 2020). At
654 the bulk level, post-vaccination effector T cell subsets did not display higher
655 exhaustion scores compared to pre-vaccination samples. However for COVID-19
656 patients, all samples had higher exhaustion scores compared to controls, and those
657 with severe disease displayed the highest exhaustion scores. It is possible that the high
658 exhaustion status of effector T cell subsets may be associated with functional
659 impairment (Zheng et al., 2020). Interestingly, the effector T cell subset from post-
660 vaccination showed lower cytotoxicity scores at the bulk level than those of pre-
661 vaccination. In contrast, the cytotoxicity scores of the effector T cell subset from
662 COVID-19 patients were higher than the controls with severe disease having the
663 highest cytotoxic score. Similarly, we observed that the cytotoxicity scores in each
664 subset of effector T cells were also significantly elevated after SARS-CoV-2 infection.

665 Although increased expression of pro-inflammatory cytokine genes was
666 observed in monocytes post-vaccination, this upregulation may not be adequate to
667 cause a significant increase in systemic levels of pro-inflammatory cytokines. This is
668 supported by our immunoassay results which showed no obvious increase in several
669 key pro-inflammatory cytokines (e.g., IL-6 and TNF) post-vaccination (**Fig S10**). In
670 addition, the expression level of pro-inflammatory cytokine genes after vaccination
671 was significantly lower than SARS-CoV-2 infection. These evidences suggest that
672 CoronaVac may not contribute to acute inflammation or the cytokine storm commonly
673 observed in severe COVID-19 patients (Zhou et al., 2020). Among the monocyte
674 subsets, CD14⁺ monocytes were identified as the major contributor to inflammation
675 for both immunization and SARS-CoV-2 infection. This is evidenced by: (i) a large

676 increase in CD14+ monocytes observed after vaccination and SARS-CoV-2 infection
677 (**Fig 3 and Fig S3**) (Zhou et al., 2020) and (ii) CD14+ monocytes was the largest
678 contributor to the inflammatory scores (**Fig 7**). In addition, due to rising concerns
679 about the bloodclotting side effect observed in several vaccine types, we also
680 examined several key genes (e.g., *2RX1*, *P2RY1* and *TBXA2R*) involved in platelet
681 aggregation in megakaryocytes (Sangkuhl et al., 2011). Unlike SARS-CoV-2
682 infection, our data demonstrated that the expression level of platelet aggregation-
683 associated genes were not significantly upregulated after immunization with
684 CoronaVac. This may explain the fewer number of thrombus-related adverse events
685 reported CoronaVac.

686

687 **Methods**

688 **Volunteer cohort**

689 Three male and three female healthy adults (n = 6) were admitted at the Sanya People's Hospital
690 and enrolled in the study. Peripheral blood samples were collected at 3 key timepoints (Fig. 1A):
691 pre-vaccine baseline (timepoint 1, day 0), 3 weeks following the first dose (timepoint 2, day 21),
692 which was also the same day they received the second dose, and finally, 2 weeks following the
693 second dose (timepoint 3, day 35). All six volunteers had matching samples at 3 time points. This
694 study design allowed us to investigate the kinetics of the immune responses following both
695 primary and secondary immunizations.

696 **Sample collection**

697 **Supplementary Table 1** summarizes the characteristics of individuals assessed in each assay. Full
698 cohort information is described in figure 1. The fresh blood samples for each timepoint
699 immediately underwent peripheral blood mononuclear cells (PBMCs) isolation using standard
700 density gradient centrifugation. PBMCs are typically employed to assess immune-regulatory
701 effects at the single-cell level. PBMCs were isolated using HISTOPAQUE-1077 (Sigma-Aldrich,
702 10771) solution according to the manufacturer's instructions. Briefly, 3 mL of fresh peripheral
703 blood was collected in EDTA anticoagulant tubes and subsequently layered onto HISTOPAQUE-
704 1077. After centrifugation, PBMCs remained at the plasma-HISTOPAQUE-1077 interface and

705 were carefully transferred to a new tube. Erythrocytes were removed using Red Blood Cell Lysis
706 Solution (10×) (Miltenyi, 130-094-183) and washed twice with 1× PBS (Gibco, 10010023). The
707 cell pellets were re-suspended in sorting buffer (PBS supplemented with 2% fetal bovine serum
708 (FBS, Gibco, 10099141)). Cell viability of PBMCs were assessed using the Countstar cell
709 viability detection kit and showed greater than 90% viability. PBMCs were then used in
710 immunological analysis and cell encapsulation. The 10x Genomics single-cell transcriptome
711 platform was used to generate the 5' gene expression profiles, T cell receptor (TCR) and B cell
712 receptor (BCR) data. This approach employs a commercial emulsion-based microfluidic platform
713 (Chromium 10x) that enables the generation of amplified cDNA used for both the preparation of
714 single cell RNA-seq libraries and TCR/BCR target enrichment and sequencing.

715 **Single cell RNA library preparation and sequencing**

716 Cell suspensions were barcoded through the 10x Chromium Single Cell platform using Chromium
717 Single Cell 5' Library, Gel Bead and Multiplex Kit, and Chip Kit (10x Genomics). Single-cell
718 RNA libraries were prepared using the Chromium Single Cell 5' Kit v2 (10x Genomics; PN-
719 1000263), Chromium Single Cell V(D)J Reagent kits (10x Genomics, PN-1000252(TCR), PN-
720 1000253(BCR)) according to the manufacturer's instructions. Each sequencing library was
721 generated with a unique sample index. The libraries were sequenced on the Illumina Novaseq6000
722 sequencer with a paired-end 150-bp (PE150) reading strategy. With the provided sample sheet, the
723 Cell Ranger (v.5.0.0) *mkfastq* command was used to demultiplex the flow cells' raw base call files
724 into fastq files.

725

726 **SARS-CoV-2-specific IgM/IgG ELISA and plasma cytokine detection**

727 The S-specific IgG/IgM and plasma cytokine detection were detected according to our previous
728 study (Wang et al., 2021).

729

730 **Quantification and Statistical analysis**

731 **Single-cell RNA-seq and data processing**

732 The human reference (v.GRCh38-3.0.0) was downloaded from the 10x Genomics official website
733 in Mar-2021. Raw and filtered gene expression matrices were generated for each sample using the

734 kallisto/bustools (kb v0.24.4) pipeline coupled with human GRCh38. The *kb count* command was
735 called to generate single cell feature counts for each sample by specifying the library name in the
736 argument. Then the filtered feature, barcode and matrix files were analyzed in python (v3.8.10)
737 using the anndata (ad) (v0.7.6) and scanpy (sc) (v1.7.2) packages. Data files of all 18 samples and
738 the largest dataset of Chinese PBMC COVID-19 infection (64 fresh PBMC samples from Cell
739 2021 Zhangzemin) were merged together by the *ad.concat* function. Cells and genes were filtered
740 by the *sc.pp.filter_cells* and *sc.pp.filter_genes* function for further analyses. First, genes expressed
741 at a proportion >0.1% of the cells were selected. Second, to minimize technical artifacts from low-
742 quality cells and potential doublets, cells meeting the following criteria were filtered out: (1) <
743 1000 or > 25000 unique molecular identifiers (UMIs, representing unique mRNA transcripts); (2)
744 <500 or > 5000 genes; or (3) > 10% UMIs derived from the mitochondrial genes. The scanpy's
745 external module Scrublet (Wolock et al., 2019) was called using the *sc.external.pp.scrublet*
746 function to identify potential doublets using default parameters. An automatically set threshold
747 labelled 299 cells with a *doubletScore* > 0.25 as "predicted_doublets" and were filtered out. After
748 quality control, a total of 585860 cells remained. The violin distribution and scatter plot for
749 computed quality measures including gene counts per cell, UMI counts per cell and mitochondrial
750 gene percentage are shown in Supplementary Fig 1. The gene expression matrix were normalized
751 by library size to 10,000 reads per cell by *sc.pp.normalize_total* function, so that all cells were
752 comparable in UMI counts. Next, the normalized counts were natural log transformed ($X = \log(X$
753 $+ 1)$) by *sc.pp.log1p* function. The log transformed expression values were used for downstream
754 analysis.

755 **Batch effect correction and dataset integration**

756 Gene features with high cell-to-cell variation in the data were prioritized using the
757 *sc.pp.highly_variable_genes* function (supplemental Fig 1). Briefly, the informative highly-
758 variable genes (HVGs) were selected within each sample separately and merged to select the
759 consensus set of 1,500 top-HVGs. All ribosomal and mitochondrial genes were removed from
760 HVGs as described (Cell 2021 Zhangzemin). The HVGs subset matrix extracted from the full
761 expression matrix was used for downstream integration steps. Then each gene was scaled to unit
762 variance and zero mean and clipped when values exceeded 10.

763 Integration of different datasets was conducted in the order of dimension reduction by principal
764 component analysis (PCA), batch effect correction using Harmony algorithm (Korunsky et al.
765 (2019), Fast, sensitive and accurate integration of single-cell data with Harmony) and
766 unsupervised clustering using Louvain algorithm (Traag et al., 2019). Specifically, the main axes
767 of variation was identified using the `sc.tl.pca` function with parameter `svd_solver='arpack'`.
768 Dimensionality of the datasets was reduced to 50 PCA components and fed into
769 `sc.external.pp.harmony_integrate` function implemented in the python package `harmonypy`. The
770 parameter `theta` was set as 2.5 for sample for technical covariate correction. Nearest neighbor
771 graph of cells was built using the `sc.pp.neighbors` function with batch-corrected matrix.

772 **Cell clustering and annotations**

773 Unsupervised clustering of cells was then computed by `sc.tl.louvain` at different resolutions using
774 the neighborhood relations of cells. Cluster-specific signature genes were identified using the
775 `sc.tl.rank_genes_groups` function. Cluster annotation was done manually by matching canonical
776 cell marker genes with Cluster-specific signature genes.

777 Clustering analysis of cell types consisted of two rounds. The first round (Louvain resolution = 1.2)
778 was performed on all cells and identified 10 major cell types (**Fig 1, S1**). The second round (with
779 Louvain resolution ranging from 0.3 to 1.8) was performed on CD4+/CD8+ T cells, B cells,
780 monocyte and DC cells separately to subdivide each cell type into sub-clusters. These sub-clusters
781 represented distinct immune cell lineages within each major cell type. Each sub-cluster was
782 manually analyzed by domain experts and considered as distinctive enough when they had at least
783 one highly expressed signature gene compared to other cells. The complete list of canonical
784 marker genes and cluster-specific highly expressed signatures are provided in Fig 3, 6, 8, S3, S6
785 and S11.

786 **Cell state score of cell subtypes**

787 After cluster annotation were completed, several gene sets from important immune processes were
788 used to compare overall activation level or physiological activity of cell clusters. Gene sets related
789 to cytokine storm and immune exhaustion were collected from previous literature (Nature Immun
790 2020, Cell 2021 zhangzemin) and gene sets about Response To Interferon Alpha (GO:0035455),
791 Response To Interferon Beta (GO:0035456), Acute Inflammatory Response (GO:0002526),

792 Apoptotic Signaling Pathway (GO:0097190), Leukocyte Migration (GO:0050900) were collected
793 from the MsigDB database. Cell state scores were calculated using the `sc.tl.score_genes` function
794 available in Scanpy.

795 The cell scores of the cell were defined as the average expression of the genes from the
796 predefined gene set with respect to reference genes. Comparison of the cell state score of one
797 condition versus another condition was statistically assessed using the Mann-Whitney rank test
798 (two-tail, p -value < 0.01 , adjusted using the Benjamini–Hochberg method).

799 **TCR and BCR V(D)J immune repertoire sequencing and analysis**

800 From one aliquot of the gene expression 5' libraries, full-length TCR/BCR V(D)J segments were
801 enriched from transcriptome cDNA via PCR amplification using the Chromium Single-Cell V(D)J
802 Enrichment kit according to the manufacturer's protocol. Similar to the gene expression pipeline,
803 immune repertoire preprocessing was performed using Cell Ranger (v.6.0.0) `vdj` command with
804 human `vdj` reference `vGRCh38-alt-ensembl-5.0.0`. This pipeline includes demultiplexing by
805 index and barcodes, TCR/BCR V(D)J sequence discovery and TCR/BCR clonotype assignment to
806 each cell. V(D)J immune repertoire was analyzed by the python-toolkit, Scirpy. In brief, the
807 productive chains of each cell were identified and connected with the cell's barcode information.
808 Each unique TRA(s)-TRB(s) pair was defined as a TCR clonotype and each unique IGH(s)-
809 IGK/IGL(s) pair was defined as a BCR clonotype. If one clonotype was present in at least two
810 cells, cells harboring this clonotype were considered to be clonal and the number of cells with
811 such pairs indicated the degree of clonality of the clonotype. Only cells with at least one
812 productive clonotype was used in the following analysis. The TCR/BCR downstream analysis
813 were similar for the most part. TCR/BCR data table of cells loaded by Scirpy was matched
814 together with gene expression profiles already prepared by Scanpy in the AnnData data structure.
815 Clonotypes were then clustered based on the similarity of their CDR3 amino acid sequences.
816 TCR/BCR diversity metric, containing clonotype frequency and clonotype composition, was
817 obtained using `scirpy.pl.alpha_diversity` function based on 'normalized_shannon_entropy'.

818 **Statistics**

819 The statistical analysis, visualization and method details described in this study were performed in
820 python and R and are provided with the results of the main text, in the figure legends or in the

821 above Methods sections. In all figures with significance marks, the following convention for
822 symbols indicating statistical significance were used:

823 ns: $p > 0.05$

824 *: $p \leq 0.05$

825 **: $p \leq 0.01$

826 ***: $p \leq 0.001$

827 ****: $p \leq 0.0001$

828

829 **Code availability**

830 Experimental protocols and the data analysis pipeline used in our work follow the 10X Genomics
831 and Seurat official websites. The analysis steps, functions and parameters used are described in
832 detail in the Methods section. Custom scripts for analyzing data are available upon reasonable
833 request. The software and algorithms used in this report are presented in Table S8.

834 **Funding:** This work was supported by grants from State Key Laboratory of Infectious Disease
835 Prevention and Control (2020SKLID303), Beijing Natural Science Foundation (5214023, M21005),
836 Public service development and reform pilot project of Beijing Medical Research Institute (BMR2019-
837 11), National natural science foundation of China (81970900) and Beijing Social Science Foundation
838 Project (19GLB033).

839 **Ethical approval:** This study was approved by the Ethics Committee of the Sanya People's Hospital
840 (SYPH-2021-26).

841 **Transparency declaration:** The lead author and guarantor affirm that the manuscript is an honest,
842 accurate, and transparent account of the study being reported; that no important aspects of the study
843 have been omitted; and that any discrepancies from the study as planned and registered have been
844 explained.

845 **Acknowledgments:** We thank all the participants. We gratefully acknowledge the participation of
846 Analytical BioSciences Co., Ltd. (Beijing) for the support of construction of single cell sequencing
847 Library, and thanks Miss. RanRan Gao (Analytical BioSciences), JuanJuan Yu (Analytical BioSciences)
848 and Mr. Feng Zhu (Analytical BioSciences) for her contribution.

849 **Reference**

- 850 Amanat, F., and Krammer, F. (2020). SARS-CoV-2 Vaccines: Status Report.
851 *Immunity* 52, 583-589.
- 852 Bayram, A., Demirbakan, H., Karadeniz, P.G., Erdoğan, M., and Koçer, I.
853 Quantitation of antibodies against SARS-CoV-2 spike protein after two doses of
854 CoronaVac in health care workers. *Journal of Medical Virology* *n/a*.
- 855 Cevik, M., Kuppalli, K., Kindrachuk, J., and Peiris, M. (2020). Virology,
856 transmission, and pathogenesis of SARS-CoV-2. *bmj* 371.
- 857 Chen, G., Wu, D., Guo, W., Cao, Y., Huang, D., Wang, H., Wang, T., Zhang, X., Chen, H.,
858 and Yu, H. (2020). Clinical and immunological features of severe and moderate
859 coronavirus disease 2019. *The Journal of clinical investigation* 130, 2620-2629.
- 860 Dong, Y., Dai, T., Wei, Y., Zhang, L., Zheng, M., and Zhou, F. (2020). A systematic
861 review of SARS-CoV-2 vaccine candidates. *Signal transduction and targeted
862 therapy* 5, 1-14.
- 863 Fortner, A., and Schumacher, D. (2021). First COVID-19 Vaccines Receiving the US
864 FDA and EMA Emergency Use Authorization. *Discoveries* 9.
- 865 Gao, Q., Bao, L., Mao, H., Wang, L., Xu, K., Yang, M., Li, Y., Zhu, L., Wang, N., and Lv, Z.
866 (2020). Development of an inactivated vaccine candidate for SARS-CoV-2. *Science*
867 369, 77-81.
- 868 Han, B., Song, Y., Li, C., Yang, W., Ma, Q., Jiang, Z., Li, M., Lian, X., Jiao, W., and Wang,
869 L. (2021). Safety, Tolerability and Immunogenicity of an Inactivated SARS-CoV-2
870 Vaccine (CoronaVac) in Healthy Children and Adolescents: A Randomised,
871 Double-Blind, and Placebo-Controlled, Phase 1/2 Clinical Trial.
- 872 Horns, F., Dekker, C.L., and Quake, S.R. (2020). Memory B cell activation, broad
873 anti-influenza antibodies, and bystander activation revealed by single-cell
874 transcriptomics. *Cell reports* 30, 905-913. e906.
- 875 Iversen, P.L., and Bavari, S. (2021a). Inactivated COVID-19 vaccines to make a
876 global impact. *The Lancet Infectious Diseases* 21, 746-748.
- 877 Iversen, P.L., and Bavari, S. (2021b). Inactivated COVID-19 vaccines to make a
878 global impact. *The Lancet Infectious Diseases*.
- 879 Jouan, Y., Guillon, A., Gonzalez, L., Perez, Y., Boisseau, C., Ehrmann, S., Ferreira, M.,
880 Daix, T., Jeannet, R., François, B., *et al.* (2020). Phenotypical and functional
881 alteration of unconventional T cells in severe COVID-19 patients. *Journal of
882 Experimental Medicine* 217.
- 883 Krammer, F. (2020). SARS-CoV-2 vaccines in development. *Nature* 586, 516-527.
- 884 Liu, Y., Zhang, C., Huang, F., Yang, Y., Wang, F., Yuan, J., Zhang, Z., Qin, Y., Li, X., and
885 Zhao, D. (2020). Elevated plasma levels of selective cytokines in COVID-19
886 patients reflect viral load and lung injury. *National Science Review* 7, 1003-1011.
- 887 Long, Q.-X., Liu, B.-Z., Deng, H.-J., Wu, G.-C., Deng, K., Chen, Y.-K., Liao, P., Qiu, J.-F.,
888 Lin, Y., and Cai, X.-F. (2020). Antibody responses to SARS-CoV-2 in patients with
889 COVID-19. *Nature medicine* 26, 845-848.
- 890 Mathew, D., Giles, J.R., Baxter, A.E., Oldridge, D.A., Greenplate, A.R., Wu, J.E., Alanio,
891 C., Kuri-Cervantes, L., Pampena, M.B., and D'Andrea, K. (2020). Deep immune

892 profiling of COVID-19 patients reveals distinct immunotypes with therapeutic
893 implications. *Science* 369.

894 Mehra, M.R., Desai, S.S., Kuy, S., Henry, T.D., and Patel, A.N. (2020). Cardiovascular
895 disease, drug therapy, and mortality in Covid-19. *New England Journal of*
896 *Medicine* 382, e102.

897 Muena, N.A., Garcia-Salum, T., Pardo-Roa, C., Serrano, E.F., Levican, J., Avendano,
898 M.J., Almonacid, L.I., Valenzuela, G., Poblete, E., and Strohmeier, S. (2021). Long-
899 lasting neutralizing antibody responses in SARS-CoV-2 seropositive individuals
900 are robustly boosted by immunization with the CoronaVac and BNT162b2
901 vaccines. medRxiv.

902 Neu, K.E., Guthmiller, J.J., Huang, M., La, J., Vieira, M.C., Kim, K., Zheng, N.-Y.,
903 Cortese, M., Tepora, M.E., Hamel, N.J., *et al.* (2019). Spec-seq unveils
904 transcriptional subpopulations of antibody-secreting cells following influenza
905 vaccination. *The Journal of Clinical Investigation* 129, 93-105.

906 Ni, L., Ye, F., Cheng, M.-L., Feng, Y., Deng, Y.-Q., Zhao, H., Wei, P., Ge, J., Gou, M., Li, X.,
907 *et al.* (2020). Detection of SARS-CoV-2-Specific Humoral and Cellular Immunity in
908 COVID-19 Convalescent Individuals. *Immunity* 52, 971-977.e973.

909 Ochiai, K., Maienschein-Cline, M., Simonetti, G., Chen, J., Rosenthal, R., Brink, R.,
910 Chong, A.S., Klein, U., Dinner, A.R., and Singh, H. (2013). Transcriptional
911 regulation of germinal center B and plasma cell fates by dynamical control of
912 IRF4. *Immunity* 38, 918-929.

913 Okada, T., Ngo, V.N., Ekland, E.H., Förster, R., Lipp, M., Littman, D.R., and Cyster, J.G.
914 (2002). Chemokine requirements for B cell entry to lymph nodes and Peyer's
915 patches. *The Journal of experimental medicine* 196, 65-75.

916 Okba, N.M., Müller, M.A., Li, W., Wang, C., GeurtsvanKessel, C.H., Corman, V.M.,
917 Lamers, M.M., Sikkema, R.S., De Bruin, E., and Chandler, F.D. (2020). Severe acute
918 respiratory syndrome coronavirus 2- specific antibody responses in coronavirus
919 disease patients. *Emerging infectious diseases* 26, 1478.

920 Pène, J., Gauchat, J.-F., Lécart, S., Drouet, E., Guglielmi, P., Boulay, V., Delwail, A.,
921 Foster, D., Lecron, J.-C., and Yssel, H. (2004). Cutting edge: IL-21 is a switch factor
922 for the production of IgG1 and IgG3 by human B cells. *The Journal of Immunology*
923 172, 5154-5157.

924 Poland, G.A., Ovsyannikova, I.G., and Kennedy, R.B. (2020). SARS-CoV-2 immunity:
925 review and applications to phase 3 vaccine candidates. *The Lancet*.

926 Raju, S., Kometani, K., Kurosaki, T., Shaw, A.S., and Egawa, T. (2018). The adaptor
927 molecule CD2AP in CD4 T cells modulates differentiation of follicular helper T
928 cells during chronic LCMV infection. *PLoS pathogens* 14, e1007053.

929 Reimer, D., Lee, A.Y., Bannan, J., Fromm, P., Kara, E.E., Comerford, I., McColl, S.,
930 Wiede, F., Mielenz, D., and Körner, H. (2017). Early CCR6 expression on B cells
931 modulates germinal centre kinetics and efficient antibody responses.
932 *Immunology and cell biology* 95, 33-41.

933 Ren, X., Wen, W., Fan, X., Hou, W., Su, B., Cai, P., Li, J., Liu, Y., Tang, F., and Zhang, F.
934 (2021). COVID-19 immune features revealed by a large-scale single-cell
935 transcriptome atlas. *Cell* 184, 1895-1913. e1819.

- 936 Sangkuhl, K., Shuldiner, A.R., Klein, T.E., and Altman, R.B. (2011). Platelet
937 aggregation pathway. *Pharmacogenet Genomics* 21, 516-521.
- 938 Shaffer, A., Shapiro-Shelef, M., Iwakoshi, N.N., Lee, A.-H., Qian, S.-B., Zhao, H., Yu, X.,
939 Yang, L., Tan, B.K., and Rosenwald, A. (2004). XBP1, downstream of Blimp-1,
940 expands the secretory apparatus and other organelles, and increases protein
941 synthesis in plasma cell differentiation. *Immunity* 21, 81-93.
- 942 Shervani, Z., Khan, I., Khan, T., and Qazi, U.Y. (2020). COVID-19 Vaccine. *Advances*
943 *in Infectious Diseases* 10, 195.
- 944 Shi, W., Liao, Y., Willis, S.N., Taubenheim, N., Inouye, M., Tarlinton, D.M., Smyth,
945 G.K., Hodgkin, P.D., Nutt, S.L., and Corcoran, L.M. (2015). Transcriptional profiling
946 of mouse B cell terminal differentiation defines a signature for antibody-
947 secreting plasma cells. *Nature immunology* 16, 663-673.
- 948 Tan, L., Wang, Q., Zhang, D., Ding, J., Huang, Q., Tang, Y.-Q., Wang, Q., and Miao, H.
949 (2020). Lymphopenia predicts disease severity of COVID-19: a descriptive and
950 predictive study. *Signal transduction and targeted therapy* 5, 1-3.
- 951 Tanriover, M.D., Doğanay, H.L., Akova, M., Güner, H.R., Azap, A., Akhan, S., Köse, Ş.,
952 Erdiñç, F.Ş., Akalin, E.H., and Tabak, Ö.F. (2021). Efficacy and safety of an
953 inactivated whole-virion SARS-CoV-2 vaccine (CoronaVac): interim results of a
954 double-blind, randomised, placebo-controlled, phase 3 trial in Turkey. *The Lancet*.
- 955 Wang, N.S., McHeyzer-Williams, L.J., Okitsu, S.L., Burris, T.P., Reiner, S.L., and
956 McHeyzer-Williams, M.G. (2012). Divergent transcriptional programming of
957 class-specific B cell memory by T-bet and ROR α . *Nature immunology* 13, 604.
- 958 Wang, Y., Wang, X., Luu, L.D.W., Chen, S., Jin, F., Wang, S., Huang, X., Wang, L., Zhou,
959 X., and Chen, X. (2021). Proteomic and metabolomic signatures associated with
960 the immune response in healthy individuals immunized with an inactivated
961 SARS-CoV-2 vaccine. medRxiv.
- 962 Wilk, A.J., Rustagi, A., Zhao, N.Q., Roque, J., Martínez-Colón, G.J., McKechnie, J.L.,
963 Ivison, G.T., Ranganath, T., Vergara, R., Hollis, T., *et al.* (2020). A single-cell atlas of
964 the peripheral immune response in patients with severe COVID-19. *Nature*
965 *Medicine* 26, 1070-1076.
- 966 Wu, Z., Hu, Y., Xu, M., Chen, Z., Yang, W., Jiang, Z., Li, M., Jin, H., Cui, G., and Chen, P.
967 (2021). Safety, tolerability, and immunogenicity of an inactivated SARS-CoV-2
968 vaccine (CoronaVac) in healthy adults aged 60 years and older: a randomised,
969 double-blind, placebo-controlled, phase 1/2 clinical trial. *The Lancet Infectious*
970 *Diseases*.
- 971 Zhang, J.-Y., Wang, X.-M., Xing, X., Xu, Z., Zhang, C., Song, J.-W., Fan, X., Xia, P., Fu, J.-
972 L., and Wang, S.-Y. (2020). Single-cell landscape of immunological responses in
973 patients with COVID-19. *Nature immunology* 21, 1107-1118.
- 974 Zhang, Y., Zeng, G., Pan, H., Li, C., Hu, Y., Chu, K., Han, W., Chen, Z., Tang, R., and Yin,
975 W. (2021). Safety, tolerability, and immunogenicity of an inactivated SARS-CoV-2
976 vaccine in healthy adults aged 18–59 years: a randomised, double-blind, placebo-
977 controlled, phase 1/2 clinical trial. *The Lancet infectious diseases* 21, 181-192.
- 978 Zheng, H.-Y., Zhang, M., Yang, C.-X., Zhang, N., Wang, X.-C., Yang, X.-P., Dong, X.-Q.,
979 and Zheng, Y.-T. (2020). Elevated exhaustion levels and reduced functional

980 diversity of T cells in peripheral blood may predict severe progression in COVID-
981 19 patients. *Cellular & molecular immunology* 17, 541-543.
982 Zhou, Y., Fu, B., Zheng, X., Wang, D., Zhao, C., Qi, Y., Sun, R., Tian, Z., Xu, X., and Wei,
983 H. (2020). Pathogenic T-cells and inflammatory monocytes incite inflammatory
984 storms in severe COVID-19 patients. *National Science Review* 7, 998-1002.
985

986 **Figure legends**

987 **Fig 1. Study design and overall results of single-cell transcriptomic profiling of PBMCs**
988 **isolated from vaccine recipients without COVID-19 infection.**

989 **A.** A schematic diagram of the overall study design. The PBMCs from six recipients, 3 male and 3
990 female adults, and across three conditions were subjected to scRNA-seq gene expression profiling,
991 TCR and BCR profiling analyses. The data set was integrated with a published COVID-19
992 scRNA-seq data set comprised of 64 fresh PBMC samples.

993 **B.** Cell populations identified and 2-D visualization. The UMAP projection of 180k single cell
994 transcriptomes from NJ (n = 6), FJ (n = 6) and SJ (n = 6) samples, showing the presence of 10
995 major clusters and 27 smaller clusters with their respective colors. Each dot corresponds to a
996 single cell, colored according to the annotated major cell type (left panel) or subcelltype (right
997 panel). **C.** Canonical single cell RNA markers were used to label major clusters by cell identity as
998 expression level on the UMAP plot. Cells are colored according to log transformed and
999 normalized expression levels of twelve genes (CD3D, CD8A, CD40LG, etc.).

1000 **D.** Expression distribution of cell identity specific RNA markers of vaccine cohort samples. The
1001 rows represent 10 cell clusters labeled with different colors and the columns represent log
1002 transformed gene expression of the RNAs. The distribution of a gene in a cluster is shown as one
1003 small violin plot.

1004 **E.** Similar to **Fig 1B**, Cell populations identified and 2-D visualization of 410k single cell
1005 transcriptomes from Cont (Control), Conv (Convalescence), Mild (Mild), and Seve (Severe)
1006 samples from Ren et al..

1007

1008 **Fig 2. Comparison of cell composition across sample groups.**

1009 **A.** UMAP projection of the single cells from NJ, FJ and SJ conditions. Each dot corresponds to a
1010 single cell, colored by its major cell type.

1011 **B.** Average proportion of each major cell type derived from NJ, FJ and SJ groups.

1012 **C.** Proportion of each major cell type derived from each NJ, FJ and SJ individual sample.

1013 **D.** The box plot shows cell compositions of NJ, FJ and SJ conditions at a single sample level.
1014 Condition preference of each cluster compared side by side. y axis, percentage of cell types. Boxes
1015 are colored by conditions. Each plot panel represents one cell type.

1016 **E.** Average proportion of each major cell type derived from Cont, Conv, Mild, and Seve conditions
1017 from the COVID-19 infection cohort.

1018 **F.** Proportion of each major cell type derived from individual samples of Cont, Conv, Mild, and
1019 Seve groups from the COVID-19 infection cohort

1020 **G.** The box plot shows cell compositions of Cont, Conv, Mild, and Seve conditions from the
1021 COVID-19 infection cohort at a single sample level.

1022 In 2D and 2G, all pairwise differences with $P < 0.05$ using two-sided unpaired Mann–Whitney U-
1023 test are marked to show significance levels.

1024

1025 **Fig 3. Characterization of B cell composition differences in individuals across vaccination**
1026 **and infection conditions**

1027 **A.** UMAP projection of all B cells from NJ, FJ and SJ conditions. Each dot corresponds to a single
1028 cell, colored by its cell subtype.

1029 **B.** Expression levels of canonical B cell RNA markers were used to identify and label major cell

1030 clusters on the UMAP plot. Cells are colored according to log transformed and normalized
1031 expression levels of eight genes. Cells are from NJ, FJ and SJ conditions
1032 **C.** Average proportion of each B cell subtype derived from NJ, FJ and SJ groups.
1033 **D.** Proportion of each B cell subtype derived from NJ, FJ and SJ individual samples.
1034 **E.** The box plot shows the composition of B cells before (NJ) and after vaccination (FJ, SJ) at a
1035 single sample level.
1036 **F.** UMAP projection of all B cells from Cont, Conv, Mild and Seve conditions. Each dot
1037 corresponds to a single cell, colored by its cell subtype.
1038 **G.** Proportion of each B cell subtype derived from Cont, Conv, Mild and Seve individual samples.
1039 **H.** Antibody levels of IgM and IgG at NJ, FJ and SJ conditions in serum.
1040 **I.** The composition of Ig classes in the vaccine cohort identified by BCR single cell sequencing.
1041 **J.** The composition of Ig classes in the COVID-19 infected cohort identified by BCR single cell
1042 sequencing.
1043 All pairwise differences with $P < 0.05$ using two-sided unpaired Mann–Whitney U-test are marked
1044 to show significance levels.
1045
1046 **Fig 4. Characterization of gene expression differences in B cells in individuals across**
1047 **vaccination and infection conditions.**
1048 **A.** GO enrichment analysis of DEGs identified by comparing before- and after- vaccination
1049 conditions. DEGs refer to genes with Benjamini–Hochberg adjusted P value (two-sided unpaired
1050 Mann–Whitney U-test) ≤ 0.01 and average log₂ fold change ≥ 1 in both FJ/NJ and SJ/NJ
1051 comparisons.
1052 **B.** Violin plots of B cell expression activities in three vaccine conditions. Cells are grouped and
1053 colored by conditions. Y axis represents the normalized expression score of gene sets related to
1054 B_CELL_ACTIVATION_INVOLVED_IN_IMMUNE_RESPONSE (GO:0002312) and
1055 B_CELL_ACTIVATION (GO:0042113)
1056 **C.** Dot plots of the gene expression level of naïve B cells in three vaccine conditions. Rows
1057 represent conditions; columns represent genes. Dots are colored by mean expression levels in each
1058 condition.
1059 **D.** (Left) Dot plots of *IL4R* and *IL21R* expression level of naïve B cells between pre-vaccination
1060 and post-vaccination. Rows represent conditions; columns represent genes. Dots are colored by
1061 mean expression levels in each condition. (Right) Violin plots show the expression level of the
1062 two genes in before- and after- vaccination conditions.
1063 **E.** Violin plots of the expression level of *IL4R* and *IL21R* genes in naïve B cells, activated B cells
1064 and memory B cells.
1065 **F.** Dot plots of gene expression level of memory B and intermediate transition memory B cells in
1066 vaccine cohort. Rows represent genes (*TBX21*, *ZEB2*, *TFEC*, *ZBTB32*, *YBX3*); columns represent
1067 B cell subtypes. Dots are colored by mean expression levels in each group.
1068 **G.** *PRDM1*, *XBPI1*, *IRF4* gene expression level of activated B cells and other B cells in the vaccine
1069 cohort. Dot plots (Left) and violin plots (Right) are used for visualization.
1070 **H.** *PAX5*, *BCL6* and *BACH2* gene expression level of B cells in before- and after-vaccination
1071 conditions. Dot plots (Left) and violin plots (Right) are used for visualization.
1072 **I.** *CXCR5*, *CXCR4* and *CCR6* gene expression level of B cells in before- and after-vaccination
1073 conditions. Dot plots (Left) and violin plots (Right) are used for visualization.

1074 **J.** Gene expression level of HLA-II genes in B cells in before- and after-vaccination conditions.
1075 Dot plots (Left) show individual genes and violin plots (Right) show normalized average
1076 expression of the HLA-II gene set.

1077 **K.** Gene expression level of HLA-II genes in B cells in Cont, Conv, Mild and Seve conditions.
1078 Dot plots (Left) show individual genes and violin plots (Right) show normalized average
1079 expression of the HLA-II gene set.

1080 All pairwise differences with $P < 0.05$ using two-sided unpaired Mann–Whitney U-test are marked
1081 to show significance levels.

1082

1083 **Fig 5. Changes in BCR clones and selective usage of V(D)J genes.**

1084 **A.** UMAP projection of B cells derived from PBMCs. Cells are colored by conditions (Panel 1), B
1085 cell subtypes (Panel 2), if BCR detection was successful (Panel 3) and clone-type expansion size
1086 (panel 4)

1087 **B.** Pie graph showing the distribution of IGHA, IGHD, IGHG and IGHM in B cells and plasma
1088 cells.

1089 **C.** Box plot showing the percentages IGHA, IGHD, IGHG and IGHM in B cells and plasma cells
1090 under each condition.

1091 **D.** Pie graph showing the distribution of light chain IGK and IGL in B cells and plasma cells
1092 under each condition.

1093 **E.** Stacked bar plots showing the clone state of each B cell subtype in each condition.

1094 **F.** Heat maps showing differential IGH/K/L rearrangement. Prevalent IGHV-IGHJ combination
1095 pairs (left) and IGKV-IGKJ combination pairs (right) are compared across conditions. Usage
1096 percentage are sum normalized by column.

1097 **H.** Box plot showing the alpha diversity of clonotypes in each PBMC sample. Data points are
1098 colored by condition.

1099 **I.** Density curve plots showing the distribution shift of IGK/L and IGH chain CDR3 region length
1100 in BCR clone types for each condition.

1101

1102 **Fig 6. Characterization of innate cell composition differences in individuals across**
1103 **vaccination and infection conditions.**

1104 **A.** UMAP projection of all innate cells from NJ, FJ and SJ conditions. Each dot corresponds to a
1105 single cell, colored by its cell subtype.

1106 **B.** Expression levels of canonical innate cell RNA markers were used to identify and label major
1107 cell clusters on the UMAP plot. Cells are colored according to log transformed and normalized
1108 expression levels of eight genes. Cells are from NJ, FJ and SJ conditions.

1109 **C.** Average proportion of each innate cell subtype derived from NJ, FJ and SJ groups.

1110 **D.** Proportion of each innate cell subtype derived from NJ, FJ and SJ individual samples.

1111 **E.** The box plot shows the composition of innate cells in NJ, FJ and SJ conditions at a single
1112 sample level.

1113 **F.** UMAP projection of all innate cells from Cont, Conv, Mild, and Seve conditions. Each dot
1114 corresponds to a single cell, colored by its cell subtype.

1115 **G.** Proportion of each innate cell subtype derived from Cont, Conv, Mild and Seve individual
1116 samples.

1117 **H.** Proportion of each innate cell subtype derived from ContNJ(NJ), Vacc(FJ+SJ), Conv, MiSe

1118 (Mild and Seve) individual samples.
1119 All pairwise differences with $P < 0.05$ using two-sided unpaired Mann–Whitney U-test are marked
1120 to show significance levels.
1121
1122 **Fig 7. Characterization of gene expression differences in innate immune cells from vaccine**
1123 **and COVID-19 infected cohort samples.**
1124 **A**, GO enrichment analysis of DEGs identified by comparing the before and after vaccination
1125 conditions. DEGs refer to genes with Benjamini–Hochberg adjusted P value (two-sided unpaired
1126 Mann–Whitney U-test) ≤ 0.01 and average \log_2 fold change ≥ 1 in both
1127 FJ/NJ and SJ/NJ comparisons.
1128 **B, C and D**, Expression activity of IFN-alpha, apoptosis and migration pathways in innate
1129 immune cells of NJ, FJ, SJ, Cont, Conv, Mild and Seve conditions shown as violin plots and
1130 colored by sample conditions.
1131 **E**, Heatmap dot plot of HLA-II gene expression in innate immune cells of NJ, FJ, and SJ
1132 conditions
1133 **F**, Heatmap dot plot of HLA-II gene expression in innate immune cells of Cont, Conv, Mild and
1134 Seve conditions
1135 **G**, Violin plot showing normalized expression levels of *P2RX1*, *TBXA2R* and *P2RY1* in
1136 megakaryocytes (Mega) from NJ and Vaccine (FJ+SJ) conditions
1137 **H**, Violin plot of normalized expression of *P2RX1*, *TBXA2R* and *P2RY1* in megakaryocytes (Mega)
1138 from Cont, Mild and Seve conditions
1139 **I**, Expression activity of inflammatory pathways in monocytes from NJ, FJ and SJ conditions
1140 shown as box plots. Boxes are colored by sample conditions.
1141 **J**, Expression activity of inflammatory pathways in monocytes from Cont, Conv, Mild and Seve
1142 conditions shown as box plots. Boxes are colored by sample conditions.
1143 **K**, Expression activity of inflammatory pathways in monocytes from NJ, Vacc, Cont, Conv, Mild
1144 and Seve conditions shown as violin plots. Violins are colored by sample conditions.
1145 **L**, Pie graph of relative percentage for CD14+monocytes, CD16+monocytes,
1146 CD14+CD16+monocytes in the vaccine and COVID-19 cohort.
1147
1148 **M**, Pie graph of inflammatory scores from CD14+monocytes, CD16+monocytes,
1149 CD14+CD16+monocytes in the vaccine and COVID-19 cohort.
1150
1151 **Fig 8. Characterization of T cell composition differences in individuals across vaccination**
1152 **and infection conditions.**
1153 **A**, UMAP projection of all T cells from NJ, FJ and SJ conditions. Each dot corresponds to a single
1154 cell, colored by its cell subtype.
1155 **B**, Expression levels of canonical T cell RNA markers were used to identify and label major cell
1156 clusters on the UMAP plot. Cells are colored according to log transformed and normalized
1157 expression levels of eight genes. Cells are from NJ, FJ and SJ conditions
1158 **C**, Average proportion of each T cell subtype derived from NJ, FJ and SJ groups.
1159 **D**, Proportion of each T cell subtype derived from NJ, FJ and SJ individual samples.
1160 **E**, The box plot shows the composition of T cells from NJ, FJ and SJ conditions at a single sample
1161 level.

1162 **F**, The box plot shows the composition of T cells from Cont, Conv, Mild and Seve conditions at a
1163 single sample level.

1164 All pairwise differences with $P < 0.05$ using two-sided unpaired Mann–Whitney U-test are marked
1165 to show significance levels.

1166

1167 **Fig 9, Characterization of gene expression differences in activated T cells from vaccine and**
1168 **COVID-19 infected cohort samples.**

1169 **A**, GO enrichment analysis of DEGs identified by comparing the before and after vaccination
1170 conditions. DEGs refer to genes with Benjamini–Hochberg adjusted P value (two-sided unpaired
1171 Mann–Whitney U-test) ≤ 0.01 and average \log_2 fold change ≥ 1 in both
1172 FJ/NJ and SJ/NJ comparisons.

1173 **B** and **C**, Expression activity of IFN-alpha pathways in activated T cells (**B**) and subtypes (**C**) of
1174 NJ and Vacc (FJ and SJ) conditions shown as box plots and are colored by sample conditions.

1175 **D**, Expression activity of IFN-alpha in activated T cells of NJ, FJ, SJ, Cont, Conv, Mild and Seve
1176 conditions shown as violin plots and colored by sample conditions.

1177 **E** and **F**, Expression activity of cytotoxicity pathways in activated T cells (**E**) and subtypes (**F**) of
1178 NJ and Vacc (FJ and SJ) conditions shown as box plots and are colored by sample conditions.

1179 **G**, Expression activity of cytotoxicity pathways in activated T cells of NJ, FJ, SJ, Cont, Conv,
1180 Mild and Seve conditions shown as violin plots and colored by sample conditions.

1181 **H** and **I**, Expression activity of exhaustion genes in activated T cells (**H**) and subtypes (**I**) of NJ
1182 and Vacc (FJ and SJ) conditions shown as box plots and are colored by sample conditions.

1183 **J**, Expression activity of exhaustion genes in activated T cells of NJ, FJ, SJ, Cont, Conv, Mild and
1184 Seve conditions shown as violin plots and colored by sample conditions.

1185 **K** and **L**, Expression activity of apoptosis pathways in T cells (**K**) and subtypes (**L**) of NJ and
1186 Vacc (FJ and SJ) conditions shown as box plots and are colored by sample conditions.

1187 **M**, Expression activity of apoptosis pathways in activated T cells of NJ, FJ, SJ, Cont, Conv, Mild
1188 and Seve conditions shown as violin plots and colored by sample conditions.

1189 **N** and **O**, Expression activity of migration pathways in activated T cells (**N**) and subtypes (**O**) of
1190 NJ and Vacc (FJ and SJ) conditions shown as box plots and are colored by sample conditions.

1191 **P**, Expression activity of migration pathways in activated T cells of NJ, FJ, SJ, Cont, Conv, Mild
1192 and Seve conditions shown as violin plots and colored by sample conditions.

1193 **Q** and **R**, Gene expression level of CD2AP (**Q**) and TNFSF14 (**R**) in activated CD4+T cells in NJ,
1194 FJ, SJ, Cont, Conv, Mild and Seve conditions. Violin plots showed normalized average expression
1195 of CD2AP (**Q**) and TNFSF14 (**R**).

1196 **S** and **T**, Gene expression level of KDM5A (**S**) and TNFSF14 (**T**) in cytotoxic CD8+T cells in NJ,
1197 FJ, SJ, Cont, Conv, Mild and Seve conditions. Violin plots showed normalized average expression
1198 of KDM5A (**S**) and TNFSF14 (**T**).

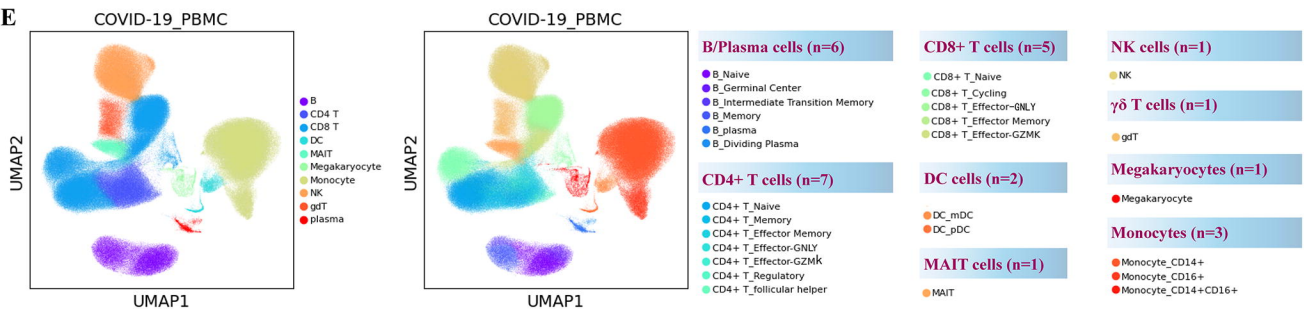
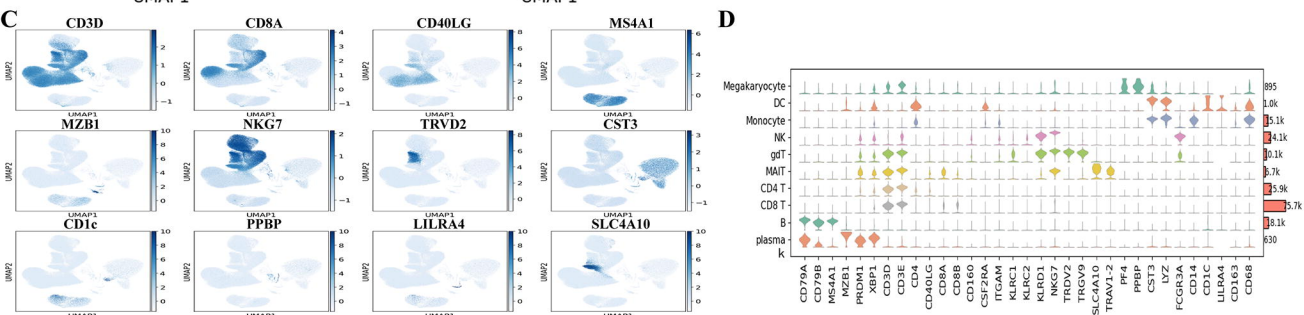
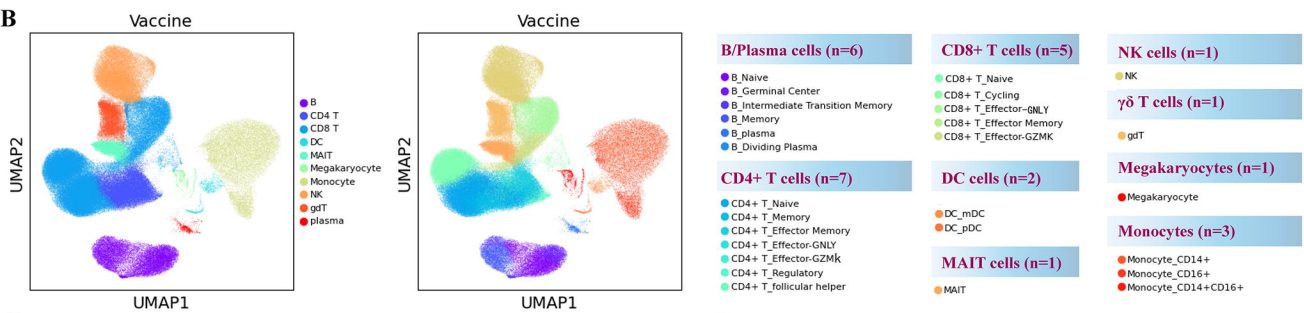
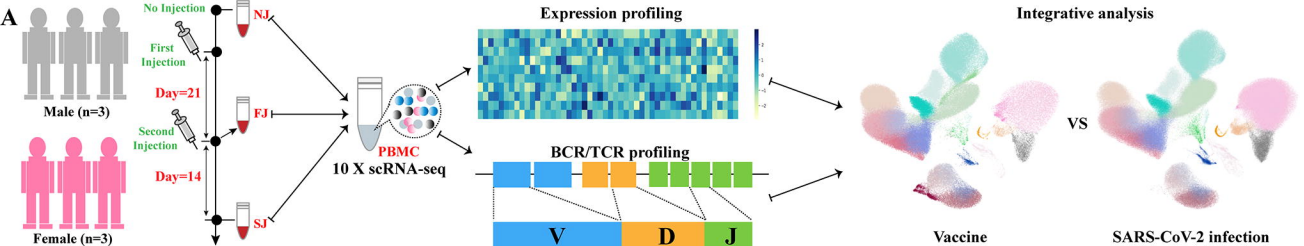
1199 All pairwise differences with $P < 0.05$ using two-sided unpaired Mann–Whitney U-test are marked
1200 to show significance levels.

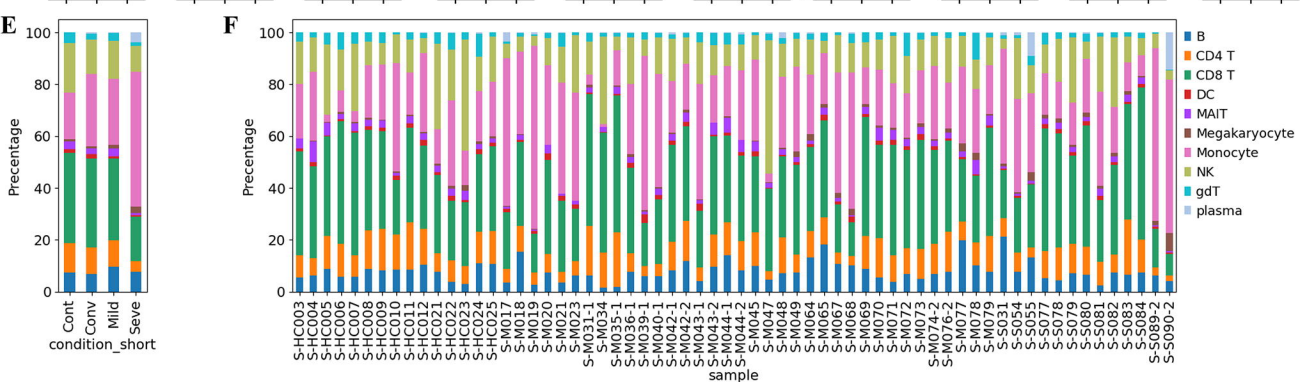
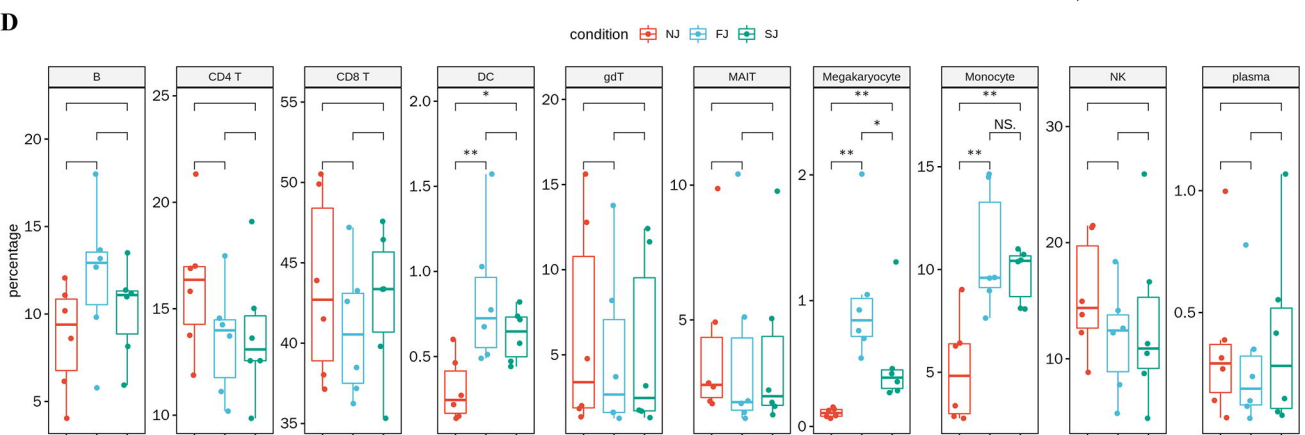
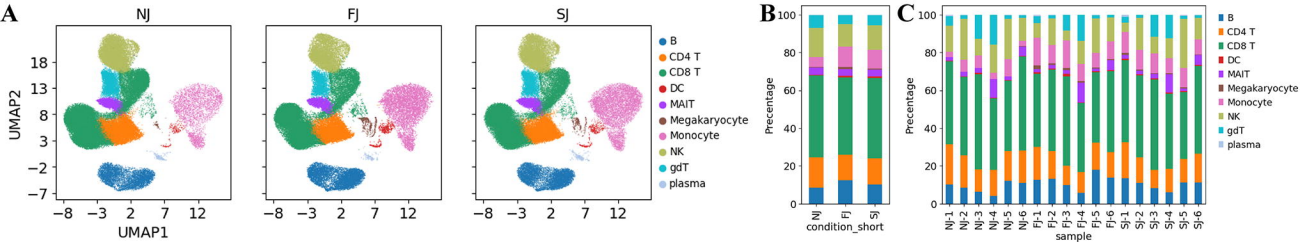
1201

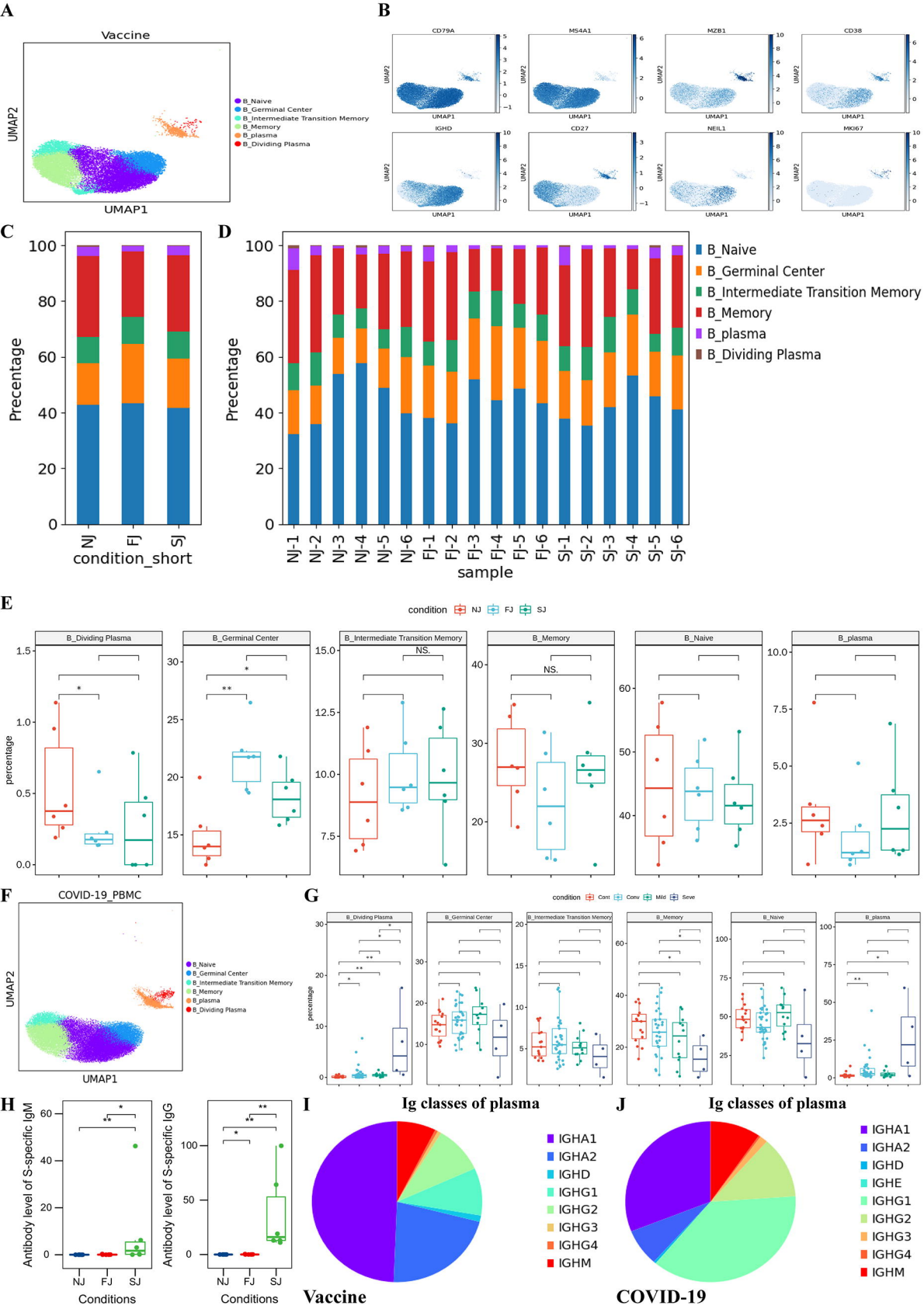
1202 **Fig 10. Changes in TCR clones and selective usage of V(D)J genes.**

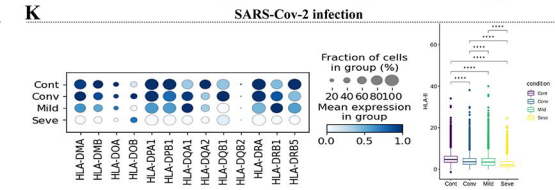
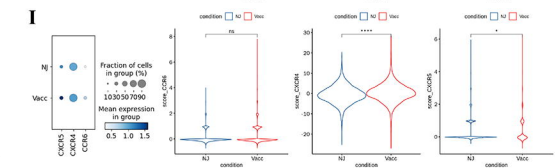
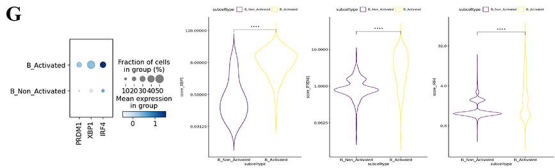
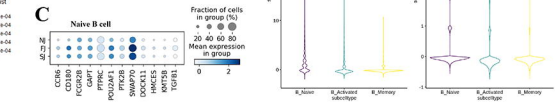
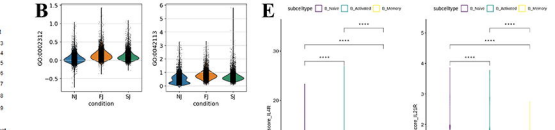
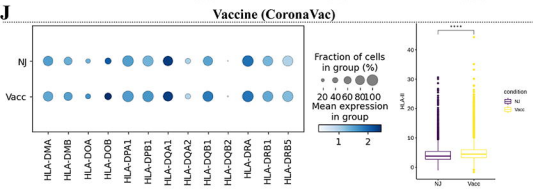
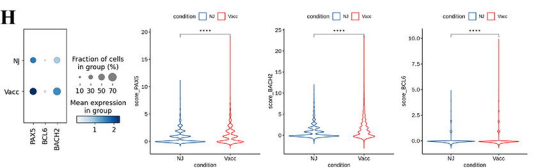
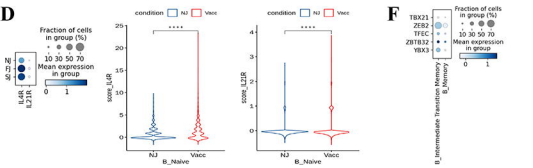
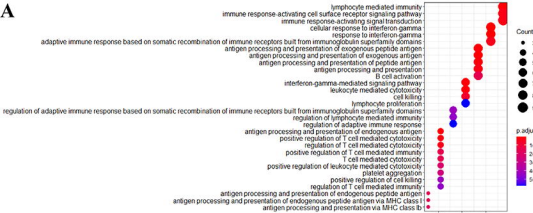
1203 **A**, UMAP projection of T cells derived from PBMCs. Cells are colored by conditions (Panel 1), T
1204 cell subtypes (Panel 2), if TCR detection was successful (Panel 3) and clonotype expansion size
1205 (panel 4).

- 1206 **B**, Stacked bar plot shows the TCR detection success rate for each T cell subtype.
1207 **C**, Histogram shows the negative correlation between the number of T cell clones and the number
1208 of cells per clonotype. Y axis is log₁₀ scaled.
1209 **D**, Pie graph showing the distribution of TRBC1 and TRBC2 in T cells under each condition.
1210 **E**, Stacked bar plots showing the clone state of each T cell subtype in each condition.
1211 **F**, Heat maps showing differential TRBV-J and TRAV-J rearrangement. Prevalent TRBV-J
1212 combination pairs (top) and TRAV-J combination pairs (bottom) are compared across conditions.
1213 Usage percentage are sum normalized by column.
1214 **G**, Density curve plots showing the distribution shift of TRA and TRB chain CDR3 region length
1215 in TCR clone types from each condition.
1216 **H**, Box plot showing TRBC1 and TRBC2 percentages in NJ, FJ, SJ, Cont, Conv, Mild and Seve
1217 conditions
1218 **I**, Box plot showing the alpha diversity of TCR clonotypes in each PBMC sample. Data points are
1219 colored by condition.

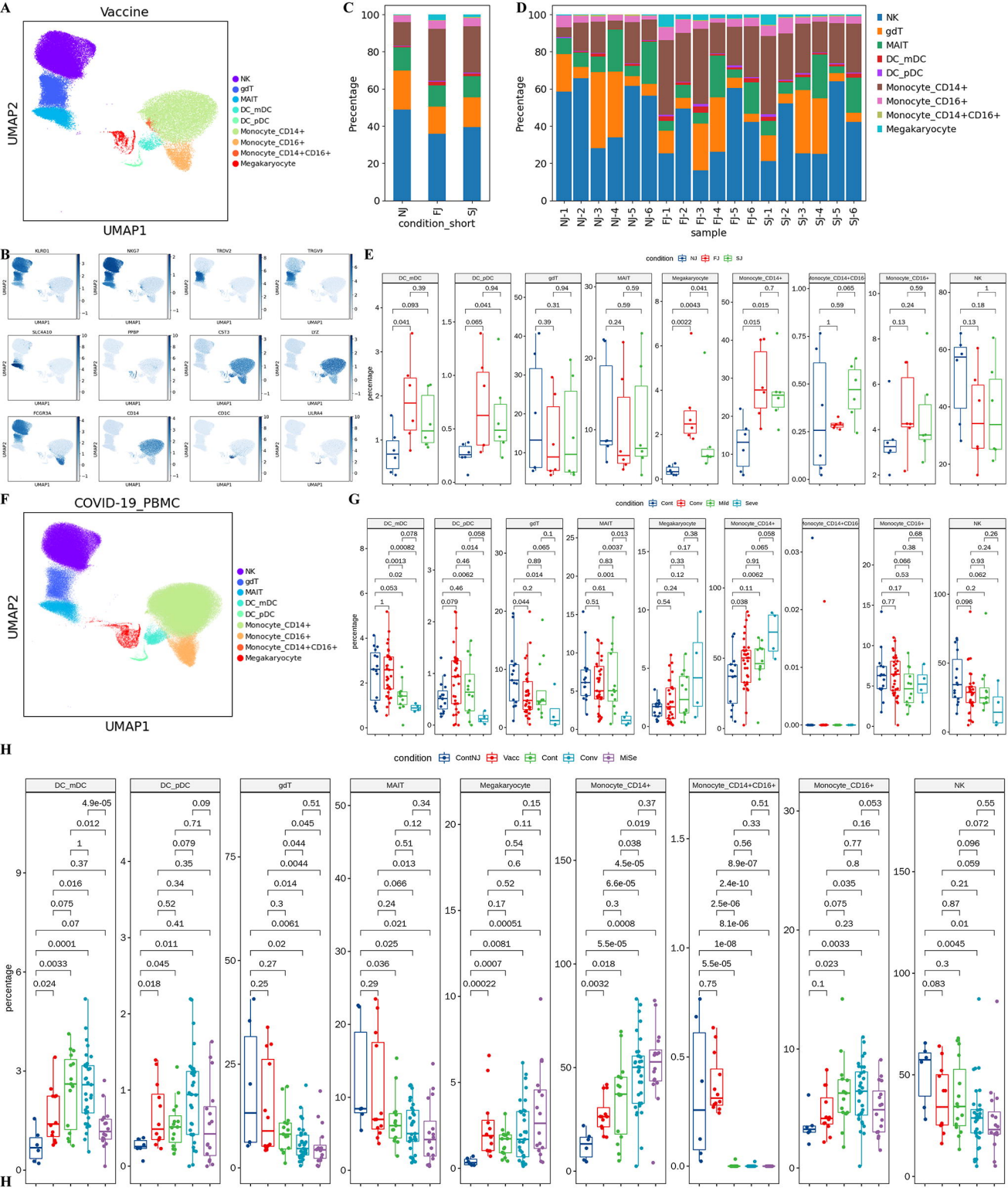


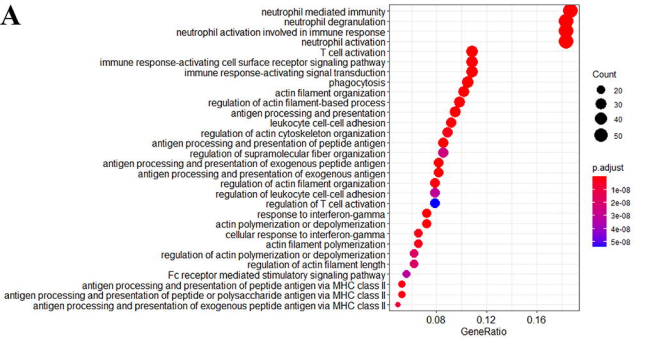




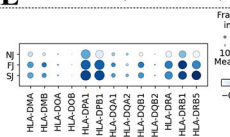




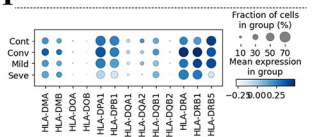




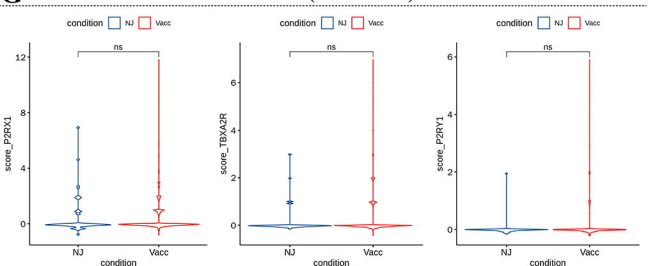
E Vaccine (CoronaVac)



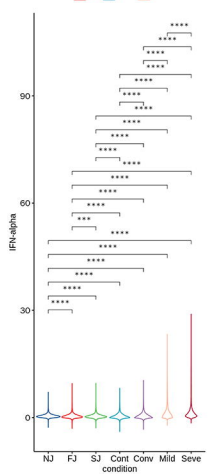
F SARS-Cov-2 infection



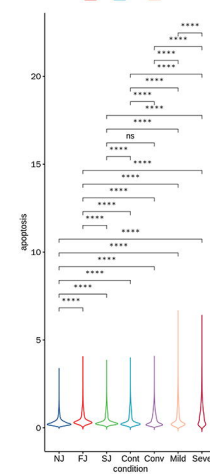
G Vaccine (CoronaVac)



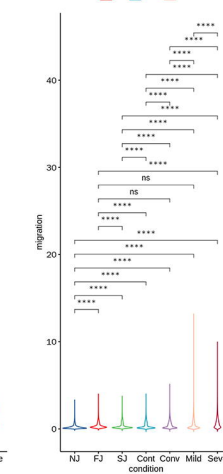
B



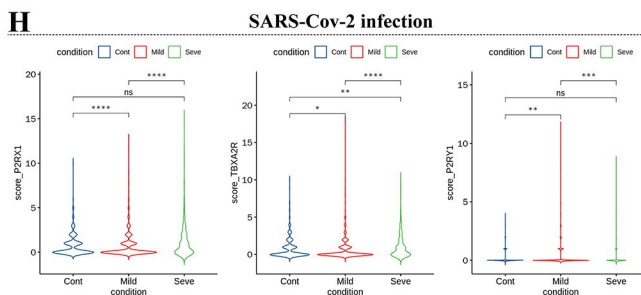
C



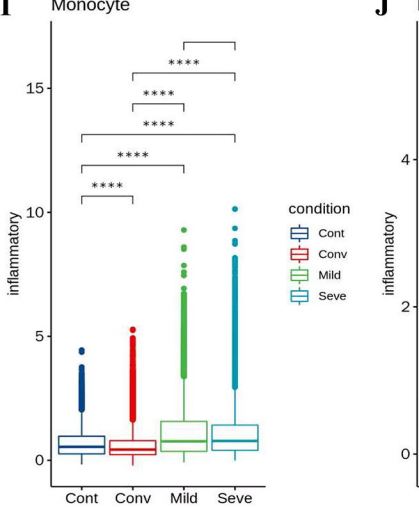
D



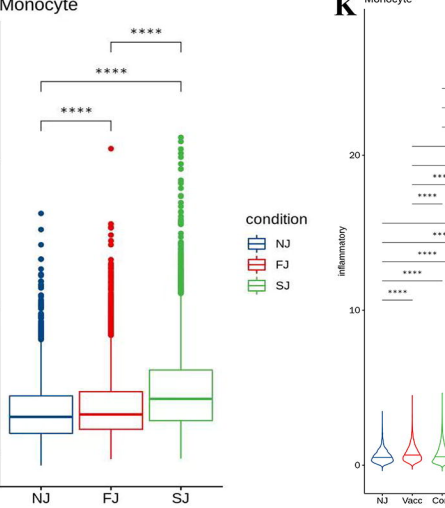
H SARS-Cov-2 infection



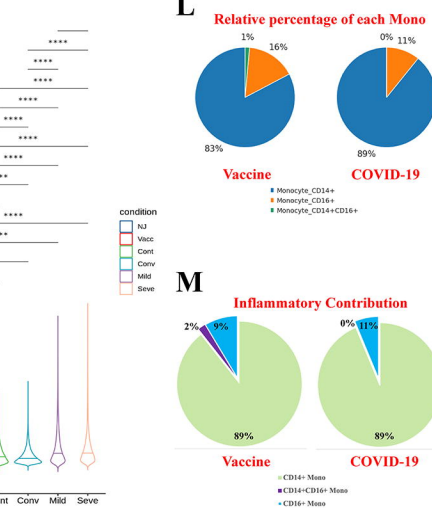
I Monocyte



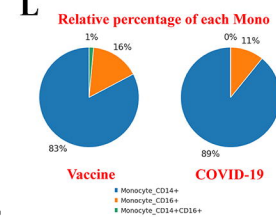
J Monocyte



K Monocyte



L Relative percentage of each Mono



M Inflammatory Contribution

